NeuroResource

Neuron

iPSC-Derived Human Microglia-like Cells to Study Neurological Diseases

Highlights

- Fully defined and efficient generation of human microglial-like cells from iPSCs
- Whole-transcriptome and functional validation of iPSC-derived microglia (iMGLs)
- Novel in vitro and in vivo applications for studying neurological diseases
- iMGLs can be used to interrogate AD gene function

Authors

Edsel M. Abud, Ricardo N. Ramirez, Eric S. Martinez, ..., Monica J. Carson, Wayne W. Poon, Mathew Blurton-Jones

Correspondence

wpoon@uci.edu (W.W.P.), mblurton@uci.edu (M.B.-J.)

In Brief

Abud et al. describe a fully defined protocol for the generation of human iPSC-derived microglia-like cells (iMGLs). Whole-transcriptome and novel functional analyses were used to validate microglial identity. iMGLs provide a platform for studying microglial function in health and disease.

Abud et al., 2017, Neuron *94*, 278–293
April 19, 2017
http://dx.doi.org/10.1016/j.neuron.2017.03.042

CellPress

CellPress

Neuron
NeuroResource

iPSC-Derived Human Microglia-like Cells to Study Neurological Diseases

Edsel M. Abud,[1,2,3] Ricardo N. Ramirez,[4] Eric S. Martinez,[1,2,3] Luke M. Healy,[5] Cecilia H.H. Nguyen,[1,2,3] Sean A. Newman,[2] Andriy V. Yeromin,[6] Vanessa M. Scarfone,[2] Samuel E. Marsh,[2,3] Cristhian Fimbres,[3] Chad A. Caraway,[3] Gianna M. Fote,[1,2,3] Abdullah M. Madany,[11] Anshu Agrawal,[7] Rakez Kayed,[8] Karen H. Gylys,[9] Michael D. Cahalan,[6] Brian J. Cummings,[2,3,10] Jack P. Antel,[5] Ali Mortazavi,[4] Monica J. Carson,[11] Wayne W. Poon,[3,*] and Mathew Blurton-Jones[1,2,3,12,*]

[1]Department of Neurobiology & Behavior
[2]Sue and Bill Gross Stem Cell Research Center
[3]Institute for Memory Impairments and Neurological Disorders
[4]Department of Developmental and Cell Biology
University of California Irvine, Irvine, CA 92697, USA
[5]Neuroimmunology Unit, Department of Neurology and Neurosurgery, Montreal Neurological Institute and Hospital, McGill University, Montreal, QC H3A 2B4, Canada
[6]Department of Physiology and Biophysics
[7]Department of Medicine, School of Medicine
University of California Irvine, Irvine, CA 92697, USA
[8]Department of Neurology, George P. and Cynthia Woods Mitchell Center for Neurodegenerative Diseases, University of Texas Medical Branch, Galveston, TX 77555, USA
[9]UCLA School of Nursing, University of California, Los Angeles, Los Angeles, CA 90095, USA
[10]Anatomy and Neurobiology, University of California Irvine, Irvine, CA 92697, USA
[11]Division of Biomedical Sciences, Center for Glia-Neuronal Interactions, University of California, Riverside, Riverside, CA 92521, USA
[12]Lead Contact
*Correspondence: wpoon@uci.edu (W.W.P.), mblurton@uci.edu (M.B.-J.)
http://dx.doi.org/10.1016/j.neuron.2017.03.042

SUMMARY

Microglia play critical roles in brain development, homeostasis, and neurological disorders. Here, we report that human microglial-like cells (iMGLs) can be differentiated from iPSCs to study their function in neurological diseases, like Alzheimer's disease (AD). We find that iMGLs develop in vitro similarly to microglia in vivo, and whole-transcriptome analysis demonstrates that they are highly similar to cultured adult and fetal human microglia. Functional assessment of iMGLs reveals that they secrete cytokines in response to inflammatory stimuli, migrate and undergo calcium transients, and robustly phagocytose CNS substrates. iMGLs were used to examine the effects of Aβ fibrils and brain-derived tau oligomers on AD-related gene expression and to interrogate mechanisms involved in synaptic pruning. Furthermore, iMGLs transplanted into transgenic mice and human brain organoids resemble microglia in vivo. Together, these findings demonstrate that iMGLs can be used to study microglial function, providing important new insight into human neurological disease.

INTRODUCTION

Microglia are the innate immune cells of the CNS and play important roles in synaptic plasticity, neurogenesis, homeostatic functions, and immune activity. Microglia also play a critical role in neurological disorders, including Alzheimer's disease (AD), highlighting the need to improve our understanding of their function in both health and disease. Yet, studying human microglia is challenging because of the rarity and difficulty in acquiring primary cells from human fetal or adult CNS tissue. Therefore, there is a pressing need to develop a renewable source of human microglia, such as from induced pluripotent stem cells (iPSCs).

The challenges of generating microglia from iPSCs are due to their unique developmental origin. Elegant lineage tracing studies show that microglia originate from yolk sac erythromyeloid progenitors (EMP) generated during primitive hematopoiesis (Ginhoux et al., 2010; Kierdorf et al., 2013; Schulz et al., 2012). EMPs further develop to early primitive macrophages that migrate into the developing neural tube and become microglial progenitors (Kierdorf et al., 2013; Prinz and Priller, 2014). Microglia progenitors then mature and develop ramified processes used to survey their environment, facilitate CNS development, modulate synaptic plasticity, and respond to CNS injury and pathology. Recently, murine studies identified key cytokines, cell receptors, and transcription factors required for microglia development and survival in vivo. These factors include IL-34 and TGFβ1 (Butovsky et al., 2014; Greter et al., 2012; Wang et al., 2012; Yamasaki et al., 2014). We hypothesized that iPSCs could be differentiated to human microglia in vitro by providing cues that mimic the environment present in the developing embryo.

The generation of patient-derived iPSCs has facilitated new opportunities to examine the relationships between genetic risk factors and disease. Recently, genome-wide association studies (GWASs) have identified several genes expressed by

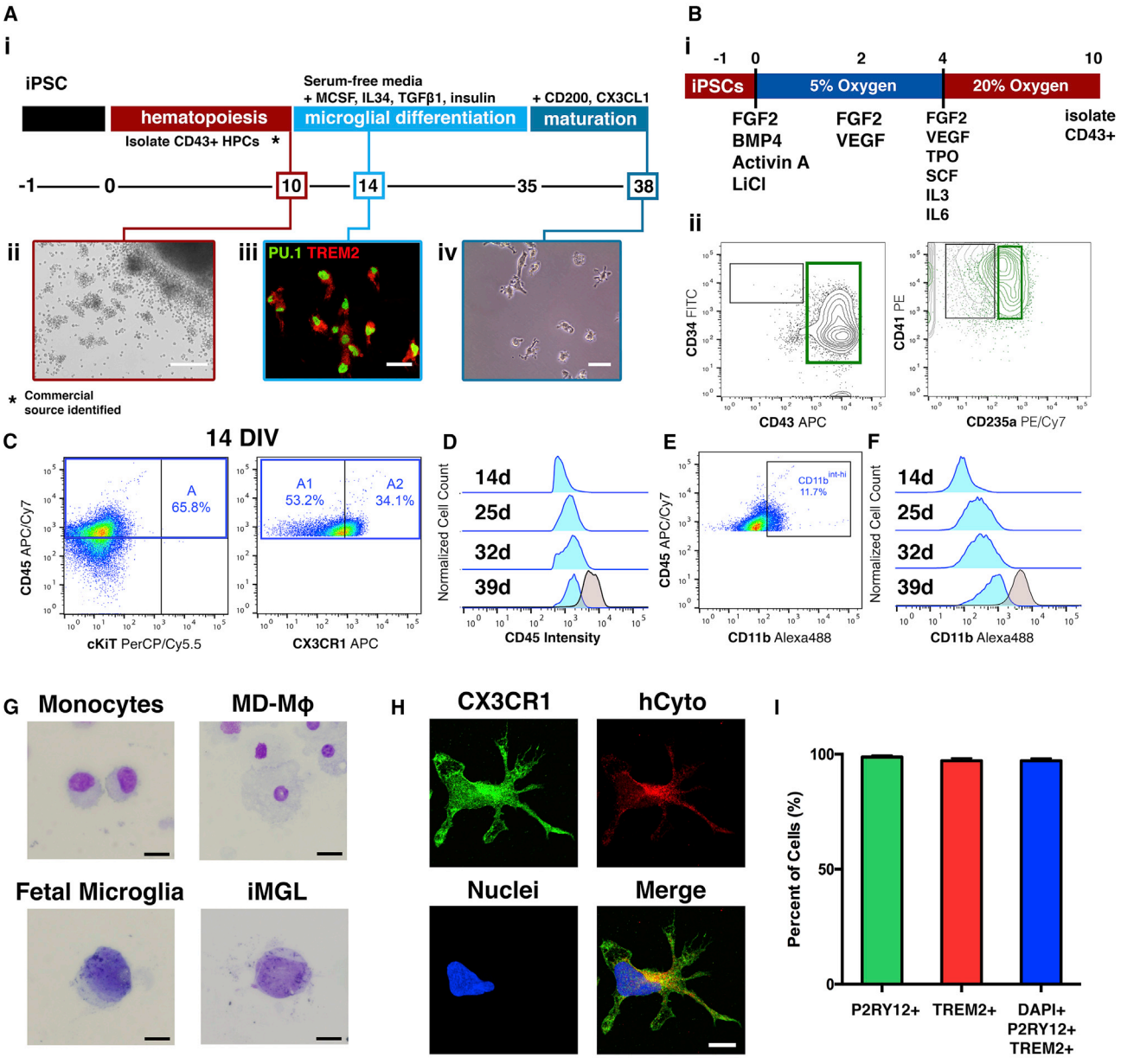

Figure 1. Differentiation of Human iPSC-Derived Microglia-like Cells

(A) Schematic of fully defined iPSC-derived microglia-like cell (iMGL) differentiation protocol. Human iPSCs are differentiated to CD43$^+$ iHPCs for 10 days and then cultured in serum-free microglia differentiation media containing human recombinant MCSF, IL-34, and TGFβ-1 (i). Differentiation is carried out for an additional 25 days after which iMGLs are exposed to human recombinant CD200 and CX3CL1 for 3 days. Representative image of iHPCs in cell culture at day 10 (ii). Scale bar, 100 μm. By day 14, iMGLs express PU.1 (green) and TREM2 (red) (iii). Scale bar, 50 μm. Representative phase contrast image of iMGL at day 38 (iv).

(B) Schematic of differentiation of iPSCs to iHPCs. Single-cell iPSCs are differentiated in a chemically defined media supplemented with hematopoietic differentiation factors and using 5% O_2 (4 days) and 20% O_2 (6 days) (i). After 10 days, CD43$^+$ iHPCs are CD235a$^+$/CD41a$^+$ (ii).

(C) iMGLs develop from CD45$^+$/CX3CR1$^-$ (A1) and CD45$^+$/CX3CR1$^+$ (A2) progenitors.

(D) CD45 fluorescence intensity shows that iMGLs (blue) maintain their CD45$^{lo\text{-}int}$ profile when compared to monocyte-derived macrophages (MD-Mφ).

(E) iMGL progenitors are CD11b^{lo} and increase their CD11b expression as they mature. At 14 DIV, a small population (~11%) of cells with CD11b$^{int\text{-}hi}$ are detected.

(F) CD11b fluorescence intensity demonstrates that CD11b expression increases as iMGLs age, resembling murine microglial progenitors identified by Kierdorf et al. (2013).

(legend continued on next page)

microglia that are associated with the risk of developing late-onset AD (LOAD), such as *TREM2* and *CD33*. The role of these genes in microglial function and AD is just beginning to be examined in mouse models, but the generation of human microglia-like cells would allow for the interrogation of human-specific genes that cannot be modeled in mice.

In AD, microglia cluster around β-amyloid plaques highlighting their inability to clear β-amyloid (Hickman et al., 2008; Liu et al., 2010). Microglia are also implicated in the neuroinflammatory component of AD etiology, including cytokine/chemokine secretion, which exacerbates disease pathology (Guillot-Sestier and Town, 2013). Furthermore, microglia-expressed AD-GWAS genes, like *TREM2* and *CD33*, likely play a role in AD progression. Thus, there is a pressing need to further our understanding of human microglia and the influence of both pathology and disease-associated genes on microglial function. Addressing this critical need, we report the effective and robust generation of human iPSC microglial-like cells (iMGLs) that resemble fetal and adult microglia and demonstrate their utility in investigating neurological diseases like AD.

RESULTS

Human Microglia-like Cells Are Generated from iPSCs

A two-step fully defined protocol was developed to efficiently generate microglia-like cells from iPSCs in just over 5 weeks (Figure 1A). This approach was used to successfully produce iMGLs from ten independent iPSC lines (Figures S1A–S1C). A critical prerequisite is the robust differentiation of iPSCs to hematopoietic progenitors (iHPCs). This recapitulates microglia ontogeny as iHPCs represent early primitive hematopoietic cells derived from the yolk sac that give rise to microglia during development (Ginhoux et al., 2010; Kierdorf et al., 2013). Our protocol (depicted in Figure 1Bi) yields primitive iHPCs that are $CD43^+/CD235a^+/CD41^+$ after 10 days (Kennedy et al., 2007; Sturgeon et al., 2014). Fluorescence-activated cell sorting (FACS) for $CD43^+$ cells reveal that our approach produces iHPCs with a >90% purity (Figure 1Bii). The resulting iHPCs resembled a commercial source (Cellular Dynamics International) and represent the hematopoietic progenitor used to generate iMGLs.

Next, $CD43^+$ iHPCs were grown in serum-free differentiation medium (formulated in house) containing CSF-1, IL-34, and TGFβ1. By day 14, cells expressed the myeloid-associated transcription factor PU.1 and the microglia-enriched protein TREM2 (Figure 1Aiii), demonstrating an early commitment toward microglial fate. Because this protocol yields large amounts of iMGLs, microglia development was studied in vitro as cells could be characterized every 4 days by flow cytometry. Day 14 early iMGLs were $c\text{-}kit^-/CD45^+$ (Figure 1C), suggesting commitment toward a myeloid lineage. Additionally, cells can be further subdivided into $CD45^+/CX3CR1^-$ (A1) and $CD45^+/CX3CR1^+$ (A2) populations, similar to developing microglial progenitors identified in vivo (Kierdorf et al., 2013). CD45 expression was consistently monitored in developing iMGLs and compared to monocyte-derived macrophages (MD-Mφ). While CD45 expression increased with maturation, levels never reached that of macrophages (Figure 1D), consistent with murine development (Kierdorf et al., 2013). A small population of iMGLs (~10%) also expressed intermediate CD11b levels by day 14 that also increased as cells matured but again never reached macrophage levels (Figures 1E and 1F).

By day 38, iMGLs resemble human microglia, but not monocytes nor macrophages, by cytospin/Giemsa staining (Figure 1G) and express many other microglial-enriched proteins, including MERTK, ITGB5, CX3CR1, TGFβR1, and PROS1 (Figures 1H; Figure S4). Like murine microglia development in vivo, iMGLs developing in vitro express PU.1, TREM2, and $CD11b^{int}/CD45^{low}$ (Figures 1Aiii and 1D–1F). As iMGLs mature in vitro, they also become more ramified, similar to microglia in vivo (Figures 1Aiv and 1H). Furthermore, purinergic receptor P2RY12 and TREM2 co-expression was enriched in iMGLs when compared to monocytes and quantification reveals that our protocol yielded iMGLs of high purity (>97.2%, n = 5) (Figure 1I; Figures S2A and S2B).

Genomic integrity was also maintained over the course of differentiation. Assessing copy number variants across all chromosomes demonstrated that extra chromosomal fragments were not acquired by iMGLs when compared to their respective iPSCs (n = 6, Figures S1D and S1E). A comparison of a representative differentiation across the entire probeset (n = 383, nCounter Human Karyotype Panel) revealed a high correlation between the iPSC and iMGL genomes ($r^2 > 0.92$, Figure S1F). Importantly, this protocol typically yielded 30–40 million iMGLs from one million iPSCs, suggesting that our approach can be readily scaled up for high content screening. All iPSC work was performed with approval from the appropriate University of California, Irvine oversight committee (see STAR Methods).

iMGLs Resemble Human Fetal and Adult Microglia

Next, the iMGL transcriptome was profiled in comparison to human primary fetal microglia (Fetal MG) and adult microglia (Adult MG). $CD14^+/CD16^-$ monocytes (CD14 M), $CD14^+/CD16^+$ inflammatory monocytes (CD16 M), myeloid dendritic cells (Blood DCs), iHPCs (Figure S2C–S2E), and iPSCs were also examined to compare iMGLs to stem cells and other myeloid molecular signatures. Correlation analysis and principal component analysis (PCA) revealed striking similarity of iMGLs (blue) to Fetal MG (orange) and Adult MG (green) (Figure 2A; Figure S3A). We confirmed that myeloid, hematopoietic, and stem cells used in correlation and PCA analyses expressed lineage-specific markers (Figure S3B). Furthermore, the first principal component PC1 (21.3% variance, Figure 2A, arrows) defines the differentiation time series from iPSC through iHPC to our iMGL cells while PC2 and PC3 define the dendritic and monocyte trajectories, respectively. Biclustering analysis using 300 microglial,

(G) Mary-Grunwald Giemsa stain of monocytes, MD-Mφ, fetal microglia, and iMGLs. Both fetal microglia and iMGL exhibit a high nucleus to cytoplasm morphology compared to monocytes and MD-Mφ. Scale bars, 16 μm.

(H) iMGLs also exhibit extended processes and express CX3CR1 (green) together with the human cytoplasmic marker (hCyto, SC121; red).

(I) Differentiation yields >97.2% purity as assessed by co-localization of microglial-enriched protein P2RY12 (green), microglial-enriched TREM2 (red), and nuclei (blue; n = 5 representative lines). See also Figures S1 and S2.

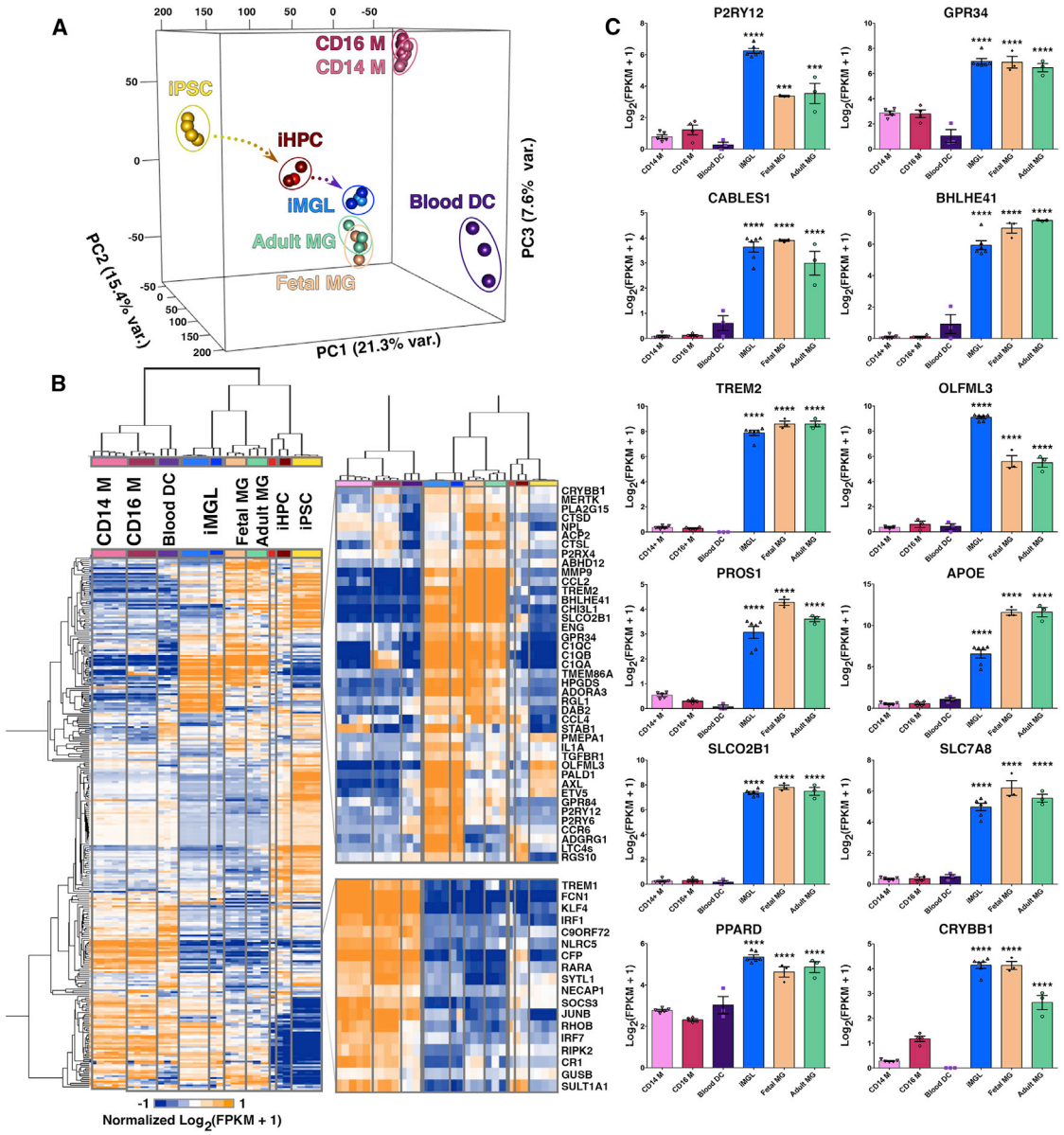

Figure 2. iMGL Transcriptome Profile Is Highly Similar to Human Adult and Fetal Microglia

(A) 3D principal component analysis (PCA) of iMGLs (blue), human adult microglia (Adult MG; green), human fetal microglia (Fetal MG; beige), $CD14^+/CD16^-$ monocytes (CD14 M; pink), $CD14^+/16^+$ monocytes (CD16 M; maroon), blood dendritic cells (Blood DC; purple), iHPCs (red), and iPSCs (yellow) (FPKM $\geq$ 1, n = 23,580 genes). PCA analysis reveals that iMGL cluster with Adult and Fetal MG and not with other myeloid cells. PC1 (21.3% var.) reflects the time series of iPSC differentiation to iHPC (yellow arrow) and then to iMGLs (blue arrow). PC2 (15.4% var.) reflects the trajectory to Blood DCs. PC3 (7.6% var.) reflects the trajectory to monocytes.

(B) Heatmap and biclustering (Euclidean distance) on 300 microglia, myeloid, and other immune-related genes (Butovsky et al., 2014; Hickman et al., 2013; Zhang et al., 2014). A pseudo-count was used for FPKM values (FPKM +1), $\log_2$-transformed, and each gene was normalized in their respective row (n = 300). Representative profiles are shown for genes up- and downregulated in both human microglia (fetal/adult) and iMGLs.

(C) Bar graphs of microglial-specific or -enriched genes measured in iMGL, Fetal and Adult MG, Blood DC, CD14 M, and CD16 M as [Log_2 (FPKM +1)] presented as mean ± SEM. Data were analyzed using one-way ANOVA followed by Tukey's corrected multiple comparison post hoc test. Statistical annotation represents greatest p value for iMGL, Fetal MG, and Adult MG to other myeloid cells. CD14 M (n = 5), CD16 M (n = 4), Blood DC (n = 3), iMGL (n = 6), Fetal MG (n = 3), and Adult MG (n = 3). *p < 0.05, **p < 0.01, ***p < 0.001, ****p < 0.0001. Complete statistical comparisons are provided in Table S1. See also Figures S2 and S3.

macrophage, and other immune-related genes adapted from previous studies (Butovsky et al., 2014; Hickman et al., 2013; Zhang et al., 2014) identified similarities between groups and highlighted common gene clusters but also uncovered differences between all groups. Again, this analysis showed that iMGLs cluster with microglia but are distinct from other myeloid

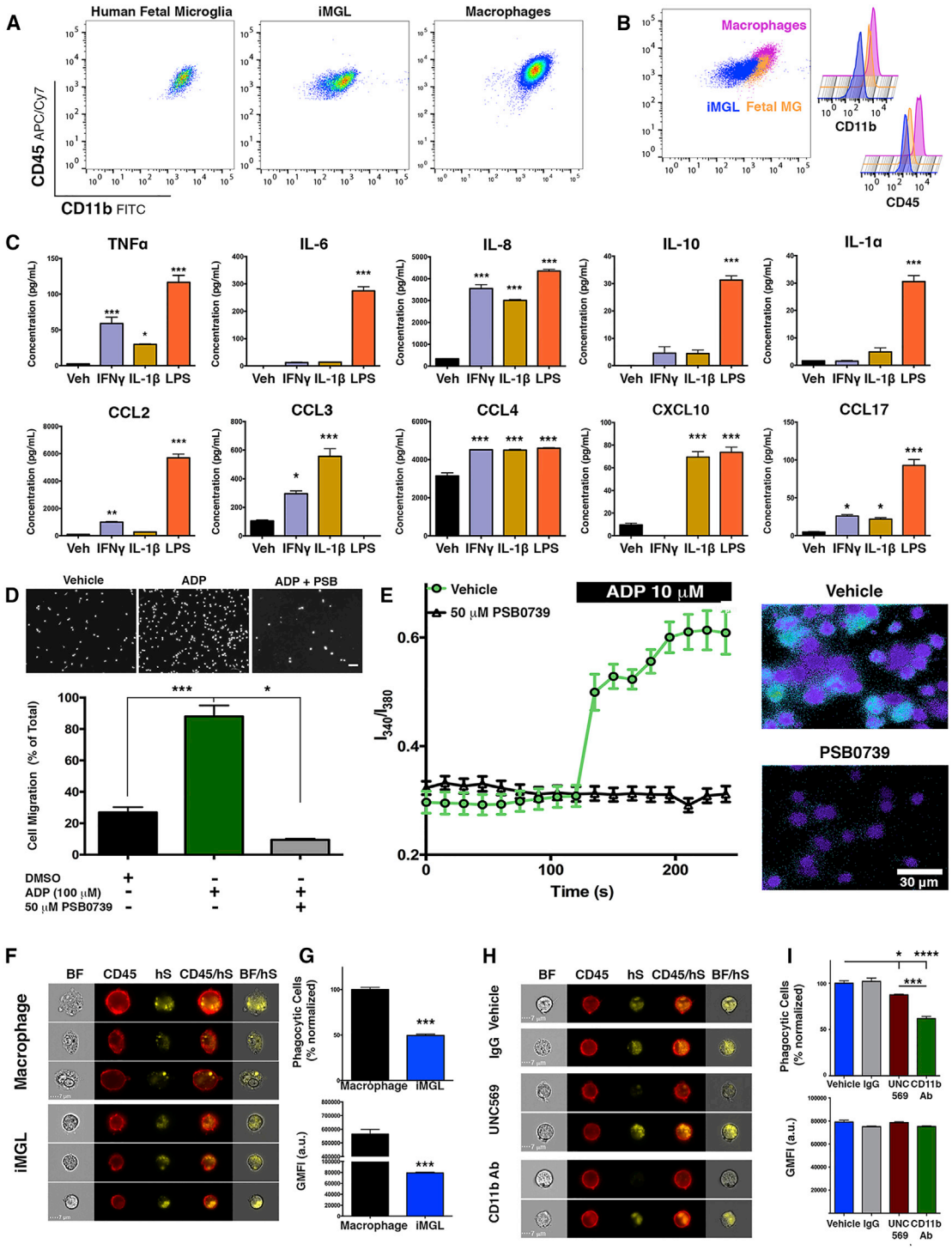

Figure 3. iMGLs Are Physiologically Functional and Can Secrete Cytokines, Respond to ADP, and Phagocytose Human Synpatosomes

(A) Flow cytometry analysis of human fetal microglia, iMGL, and macrophages.

(B) Comparative analysis shows that iMGLs (blue) are CD45$^{lo\text{-}int,}$ similar to fetal MG (orange) but different from CD45^{hi} MD-Mφ (fuchsia). Histogram of CD11b intensity (left) reveals that Fetal MG express slightly more CD11b than iMGL but less than MD-Mφ.

(C) iMGLs secrete cytokines and chemokines when stimulated for 24 hr with either IFNγ (20 ng/mL), IL-1β (20 ng/mL), or LPS (100 ng/mL) by ELISA multiplex.

(D) ADP (100 μM) induces iMGL migration in a trans-well chamber (5 μm). Pre-exposure to the P2RY12 antagonist PSB0739 (50 μM, 1 hr) completely abrogates ADP-induced iMGL migration (***p < 0.0001).

(legend continued on next page)

cells, iHPCs, and iPSCs (Figure 2B). All studies using human tissue were approved by the appropriate institutional review board (see STAR Methods).

Importantly, iMGLs, Fetal MG, and Adult MG express canonical microglial genes, such as *P2RY12*, *GPR34*, *C1Q*, *CABLES1*, *BHLHE41*, *TREM2*, *ITAM PROS1*, *APOE*, *SLCO2B1*, *SLC7A8*, *PPARD*, and *CRYBB1* (Figure 2C; Table S1). When compared to monocytes, iMGLs express the myeloid genes *RUNX1*, *PU.1*, and *CSF1R* are enriched for *P2RY12*, *OLFML3*, and *GPR34* yet do not express monocyte-specific transcription factors *IRF1*, *KLF4*, and *NR4A1* (Abdollahi et al., 1991; Hanna et al., 2011; Lavin et al., 2014) (Figures S3C–S3E). Differential analysis between iMGLs, CD14 M, and CD16 M (Figure S3F) further emphasized that iMGLs predominantly express microglial genes (greater than 2-fold change and $p < 0.001$), including *CX3CR1*, *TGFβR1*, *RGS10*, and *GAS6*, but not monocyte and macrophage genes *KLF2*, *TREM1*, *MPO*, *ITGAL*, and *ADGRE5*. At the protein level, iMGLs, like primary microglia, are $CD45^{lo}$ compared to $CD45^{hi}$ MD-Mφ and express the microglia surface proteins CX3CR1, TGFβR1, P2RY12, MERTK, PROS1, and ITGB5 (Figures S2A and S4A–S4C). Collectively, unbiased whole-transcriptome analysis and protein expression of key microglial markers strongly establishes iMGLs as a cell model that highly resembles primary human microglia that can be used to study microglia physiology and function in human health and disease.

Whole-transcriptome differential gene expression analysis revealed increased expression of 1,957 genes and 1,071 genes in iMGLs when compared to Fetal MG or Adult MG, respectively. We also observed decreased expression of 1,916 genes compared to fetal MG and 1,263 genes compared to Adult MG. Enrichment analysis between iMGLs and primary microglia show that iMGLs are enriched for pathways involving cell cycle processes, migration, microtubule cytoskeletal organization, and inflammatory response but do not differ in core myeloid gene ontology (GO) terms (Tables S4–S6). These terms reflect expected processes in which iMGLs are cued to respond to the environment and possess a capacity for renewal and maturation that have previously been reported in cultured microglia (Butovsky et al., 2014). Differential gene expression analysis between Fetal MG and Adult MG identified pathways related to responses to environment, like migration and phagocytosis regulation, but not key myeloid genes in Fetal MG. Adult MG enrichment includes electron cryomicroscopy (ECM) organization, nervous system regulation, cell adhesion, and negative regulation of cell proliferation.

Functional Validation of iMGLs

Next, iMGLs were validated as surrogates of microglia using both functional and physiological assays. By flow cytometry analysis, iMGLs were $CD11b^{int}/CD45^{lo-int}$, similar to Fetal MG (Figures 3A and 3B). Next, cytokine/chemokine secretion by iMGLs was measured following stimulation by lipopolysaccharide (LPS), IL-1β, or IFNγ. IL-1β and IFNγ are two cytokines that are elevated in AD patients and mouse models (Abbas et al., 2002; Blum-Degen et al., 1995; Marsh et al., 2016; Patel et al., 2005; Wang et al., 2015) (Figure 3C). Basally, iMGLs secrete ten of the examined cytokines at low, but detectable, levels (Table S2). However, in response to IFNγ or IL-1β, iMGLs secrete eight different chemokines, including TNFα, CCL2, CCL4, and CXCL10. As expected, iMGLs robustly responded to LPS with induction of all measured cytokines except for CCL3 (Table S2 for values). Collectively, iMGLs differentially release cytokines/chemokines based on their cell surface receptor stimuli, a finding that closely aligns with the responses observed in acutely isolated primary microglia (Rustenhoven et al., 2016).

iMGLs express the microglial-enriched purinergic receptor P2RY12, which sense extracellular nucleotides from degenerating neurons, and is critical for microglial homeostatic function (De Simone et al., 2010; Moore et al., 2015) (Figures S2A and S2B). In response to ADP, iMGLs chemotax toward ADP and produce detectable calcium transients (Figures 3D and 3E) that were both negated by a P2RY12-specific inhibitor, PSB0739. These physiological findings further underscore that iMGLs respond appropriately to stimuli and express functional surface receptors, such as P2RY12, enabling quantitative analyses of microglial physiology.

Microglia, like astrocytes, play a critical role in synaptic pruning (Aguzzi et al., 2013; Paolicelli et al., 2011; Stephan et al., 2012). Because in vitro synaptosome phagocytosis assays are an established surrogate to study pruning, the ability of iMGLs to phagocytose human synaptosomes (hS) was quantitatively assessed. In comparison to MD-Mφ, iMGL phagocytosis of pHrodo-labeled hS was less robust (Figures 3F and 3G). However, iMGLs preferentially internalized hS when compared to *E. coli* particles and normalized to MD-Mφ (Figures S4D and S4E), supporting the notion that iMGLs and microglia are more polarized toward homeostatic functions than MD-Mφ.

As iMGLs and primary microglia express both C1q and CR3 (CD11b/CD18 dimer), iMGLs were used to assess whether synaptic pruning in human microglia primarily involves this pathway as seen in mice (Hong et al., 2016a, 2016b). Using an additive-free CD11b antibody, iMGL phagocytosis of hS was significantly

(E) ADP induces calcium flux in iMGLs via P2RY12 receptors. Left: exposure to ADP leads to elevated calcium influx (I_{340}/I_{380} ratio) in vehicle group (green trace), but not in PSB0739-treated group (black trace). Right: representative images of ADP-induced calcium flux at 240 s in vehicle (top) and PSB0739 (bottom).
(F) iMGLs phagocytose human brain-derived synaptosomes (hS). Representative images captured on Amnis ImageStream display phagocytosis of hS by MD-Mφ and iMGLs.
(G) Quantification of phagocytosis shows that iMGLs internalize hS at 50% of macrophage capacity ($p < 0.0001$).
(H) Representative images of iMGL phagocytosis of hS in the presence of either a MERTK inhibitor UNC569 (top) or an anti-CD11b antibody (bottom).
(I) Top: iMGL phagocytosis of hS phagocytosis is reduced by approximately 12% (burgundy bar, $p < 0.05$) by blocking MERTK but by 40% ($p < 0.0001$, green bar) by inhibiting CR3 via CD11b blockade. Bottom: sub-analysis of iMGLs exhibiting a phagocytic event reveals similar average amounts of internalization across treatment groups ($p = 0.1165$). All histograms reported as mean ± SEM. Cytokine and migration assays one-way ANOVA, followed by Dunnett's multiple comparison post hoc test, ***$p < 0.0001$, **$p < 0.001$, *$p < 0.05$; Cytokine assay: n = 3 wells/group. Migration assay: n = 5 fields/condition. Calcium assay: vehicle (n = 37 cells), PSB0739 treated (n = 17 cells), I_{340}/I_{380} represented as mean ± SEM at each time point. Phagocytosis assay: MD-Mφ versus iMGL: unpaired t test, **$p < 0.001$, n = 3 wells/group. MERTK and CR3 assay, one-way ANOVA, followed by Tukey's multiple comparison post hoc test, ***$p < 0.0001$; n = 6 for vehicle, n = 3 wells/group. See also Figure S4.

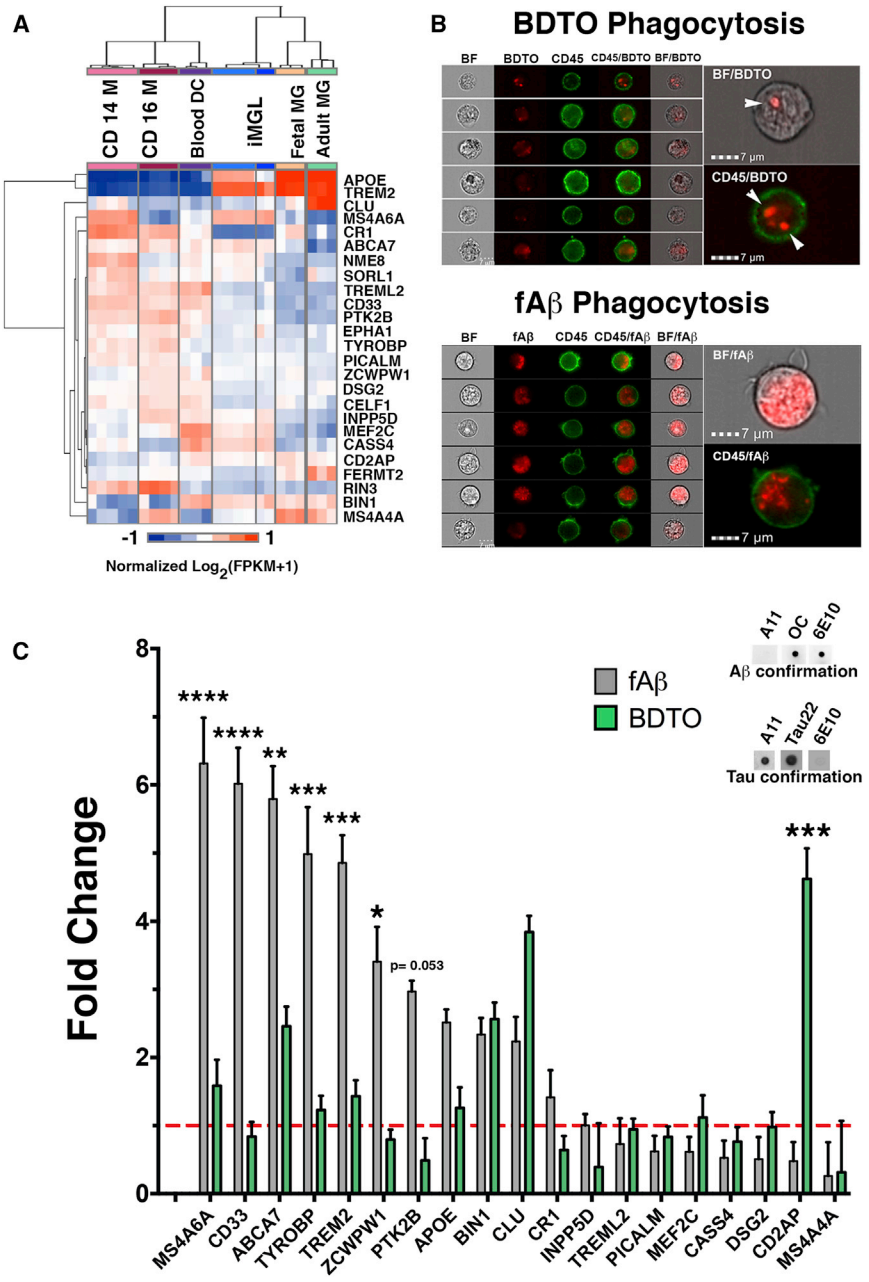

Figure 4. Alzheimer's Disease Risk Factor GWAS Genes Can Be Investigated Using iMGLs and High-Throughput Genomic and Functional Assays

(A) Heatmap of 25 immune genes with variants associated with *LOAD* reveals that major risk factors *APOE* and *TREM2* are highly expressed in iMGLs, Adult MG, and Fetal MG.

(B) iMGLs internalize fluorescent-labeled fAβ and pHrodo-dye BDTO. Representative images captured on Amnis ImageStreamX Mark II.

(C) iMGLs were exposed to unlabeled fAβ (5 $\mu g/mL^{-1}$) and BDTOs (5 μg/mL) for 24 hr, and mRNA expression of 19 GWAS genes was assessed via qPCR array. fAβ treatment elevated the expression of 10 genes above 2-fold compared to vehicle, including *MS4A6A* (6.3-fold), *CD33* (6.1-fold), *ABCA7* (5.8-fold), *TYROBP* (4.98-fold), and *TREM2* (4.85-fold). Whereas, BDTO exposure elevated the expression of four genes above 2-fold compared to vehicle. Six genes were differentially expressed in fAβ compared to BDTO. Both fAβ and BDTO preparations were confirmed via dot blot analysis with conformation structural specific antibodies for oligomers (A11), fibrils (OC), and non-structural-specific antibodies for human Aβ (6E10) and tau oligomers (Tau22). Target genes were normalized to *GAPDH* and compared to vehicle expression by ΔΔCt. Bars show expression fold mean ± SEM. Red hash bar is ΔΔCt = 1. Two-way ANOVA, followed by Sidak's multiple comparison post hoc test, ***$p < 0.0001$, **$p < 0.001$, *$p < 0.05$; n = 6 wells/group. Data represented as mean ± SEM. See also Figures S5 and S6.

reduced (−40.0%, ***$p < 0.0001$) (Figures 3H and 3I). In contrast, an inhibitor of MERTK (UNC569), also implicated in synaptic pruning, only marginally decreased iMGL hS phagocytosis (−12.6%, *$p < 0.05$) (Figures 3H and 3I). Similar to studies in murine knockout (KO) models, our data indicate that MERTK plays a minor role in human microglia-mediated synaptic pruning (Chung et al., 2013), whereas C1q/CR3 is integral for microglia-mediated synaptic pruning in humans.

Utility of iMGLs to Study Alzheimer's Disease

Impaired microglia clearance of β-amyloid (Aβ) is implicated in the pathophysiology of AD and strategies to enhance clearance of AD pathology are being actively pursued by biopharma. Therefore, we examined whether iMGLs can phagocytose Aβ or tau, two hallmark AD pathologies. Like primary microglia, iMGLs internalize fluorescently labeled fibrillar Aβ (fAβ) (Figure 4B). iMGLs also recognized and internalized pHrodo-labeled brain-derived tau oligomers (BDTOs) (Figure 4B). Fluorescence emitted indicates trafficking of pHrodo-conjugated BDTOs to the acidic lysosomal compartment, showing that iMGLs can actively ingest extracellular tau that may be released during neuronal cell death (Villegas-Llerena et al., 2016) and support recent findings that microglia may play a role in tau propagation in AD and other tauopathies (Asai et al., 2015). Together, these findings suggest that iMGLs could be utilized to identify compounds in high-throughput drug-screening assays that enhance Aβ degradation or block exosome-mediated tau release.

Microglia genes are implicated in late-onset AD, yet how they modify disease risk remains largely unknown. Thus, iMGLs were utilized to begin investigating how these genes might influence microglia function and AD risk. Hierarchical clustering using just these 25 AD-GWAS genes also demonstrates that iMGLs

resemble microglia and not peripheral myeloid cells (Figure 4A). In their investigated basal state, iMGLs and microglia express many AD-GWAS-related genes, including those without murine orthologs, i.e., *CD33*, *MS4A4A*, and *CR1*. Thus, iMGLs can be used to study how altered expression of these genes influence microglia phenotype in a way that cannot be recapitulated in transgenic mice. Therefore, iMGLs were used to investigate the influence of fAβ or BDTOs on AD-GWAS gene expression in microglia (Villegas-Llerena et al., 2016) (Figure 4C). Following fAβ exposure, iMGLs increased expression of ten genes (Table S3), including *ABCA7* (5.79 ± 0.44), *CD33* (6.02 ± 0.41), *TREM2* (4.86 ± 0.50), and *APOE* (2.52 ± 0.19), genes implicated in Aβ clearance/degradation. BDTOs increased expression of four genes, including *CD2AP* (4.62 ± 0.45), previously implicated in tau-mediated toxicity (Shulman et al., 2014). In addition, six genes were differentially elevated in fAβ compared to BDTOs (Table S3). Interestingly, *CD33*, *TYROBP*, and *PICALM*, genes more enriched in other myeloid cells at baseline, were upregulated by fAβ and BDTOs, suggesting that proteinopathies may alter microglia phenotype to resemble invading peripheral myeloid cells (Chan et al., 2007; Prinz et al., 2011; Stalder et al., 2005). In addition to AD-GWAS genes, iMGLs express other CNS disease-related genes, including *APP*, *PSEN1/2*, *HTT*, *GRN*, *TARDBP*, *LRRK2*, *C9orf72*, *SOD1*, *VCP*, and *FUS*, and therefore can likely be used to study other neurological diseases, such as amyotrophic lateral sclerosis (ALS), Huntington's disease (HD), frontal temporal dementia (FTD), and dementia with Lewy bodies (DLB), in which microglia may play a prominent role (Bachstetter et al., 2015; Crotti et al., 2014; Lui et al., 2016; O'Rourke et al., 2016) (Figure S6C).

iMGL Maturation and Homeostasis Are Modulated by a CNS Environment

Neurons, astrocytes, and endothelial cells in the brain interact with microglia to influence gene expression and function. Our differentiation protocol attempted to recapitulate CNS cues present in the brain by including signals derived from these other cell types, including CX3CL1, CD200, and TGFβ. Whole-transcriptome RNA sequencing (RNA-seq) analysis confirmed the importance of these factors for establishing microglia in vitro (Figures S5 and S6). TGFβ, a glia-derived cytokine, is needed for murine microglia development in vivo and in maintaining the microglial-specific transcriptome signature (Abutbul et al., 2012; Butovsky et al., 2014; Schilling et al., 2001). Differential gene expression analysis confirmed TGFβ's role in maintaining the human microglia transcriptome signature; 1,262 genes were differentially expressed in iMGLs with TGFβ, whereas 1,517 genes were differentially expressed in iMGLs after TGFβ removal (24 hr). Many of the differentially expressed genes are identified as core microglial signature targets, including *P2RY12*, *TGFβR1*, and *CD33*, and transcription factors *EGR1*, *ETV5*, and *APOE* (Figures S5A–S5C). Examination of gene ontology highlight neurodegenerative disease pathways, including Alzheimer's, Parkinson's, and Huntington's diseases, that are TGFβ dependent (Figure S5D). Furthermore, removal of TGFβ led to significant changes in many of the human microglia homeostatic targets also identified as AD-GWAS loci genes, including *TREM2*, *APOE*, *ABCA7*, *SPI1* (*CELF1* locus), *PILRA* (*ZCWPW1* locus), and the *HLA-DR* and *MS4A* gene clusters (Karch et al., 2016), suggesting many identified AD-GWAS genes function in the maintenance of microglia homeostasis (Figure S5E) and underscoring the utility of iMGLs to interrogate AD-GWAS gene function.

CX3CL1 and CD200 are both neuronal- and endothelial-derived cues that can further educate iMGLs toward an endogenous microglia phenotype (reviewed in Kierdorf and Prinz, 2013). To test this hypothesis, we examined how inclusion or exclusion of these factors modulates iMGL phenotype. The addition of CD200 and CX3CL1 to iMGLs increased the expression of select genes like *COMT* (Bennett et al., 2016) (Figure S5B), *CD52*, a cell surface receptor that binds Siglec10 and interacts with DAP12 as part of the microglia sensome (Hickman et al., 2013), and *HLA-DRB5*, a member of the MHC II complex implicated in AD, while maintaining similar expression levels of core-microglial genes (e.g., *P2RY12*, *TYROBP*, and *OLFML3*) and AD risk genes (Figure S6A). Importantly, we found that CD200 and CX3CL1 modulated iMGL response to CNS stimuli, such as fAβ. In the absence of CD200 and CX3CL1, fAβ stimulated the expression of AD-GWAS genes implicated in interacting with misfolded folded protein, surface receptors, or anti-apoptotic events, such as *CLU* (*APOJ*) (Yeh et al., 2016). Whereas cells exposed to these two factors responded differentially to fAβ, increasing expression of genes involved in neuronal cell surface motif recognition, or phagocytosis of CNS substrates, including *MS4A* genes, *TREM2*, *TYROBP*, *CD33*, and *ABCA7* (Bradshaw et al., 2013; Fu et al., 2016; Greer et al., 2016) (Figure S6B). These studies further support the notion that CD200-CD200R1 and/or CX3CL1-CX3CR1 axis can prime microglia to respond to neurodegenerative conditions (Prinz and Priller, 2014). Thus, exposure to soluble CNS factors, like CD200 and CX3CL1, may allow for access to microglial-specific transcriptional regulator elements (enhancers and promoters) (Gosselin et al., 2014; Lavin et al., 2014), although future studies are required to fully translate these observations.

Next, we examined whether iMGL maturation can be achieved with direct contact with the CNS environment. Therefore, iMGLs were cultured with rat hippocampal neurons (21 days in vitro [DIV]) to assess how iMGLs respond to neuronal surface cues (Figure 5A). Rat hippocampal neurons were used because they readily form synapses in culture and can be generated with limited variability. iMGLs were subsequently separated from neurons by FACS with human-specific CD45 and CD11b antibodies and profiled at the transcriptome level (Figure 5B). Differential gene expression analysis revealed that neuronal co-culturing upregulated 156 and downregulated 244 iMGL genes (Figures 5C and 5D). *FFAR2* and *COL26A1* are two genes differentially expressed in iMGLs cultured with only defined factors and indicate a developmentally primed microglia profile. In contrast, co-culturing microglia with neurons increased expression of *SIGLEC11* and *SIGLEC12*, human-specific sialic-acid binding proteins that interact with the neuronal glycocalyx, function in neuroprotection, and suppress pro-inflammatory signaling, and thus maintain a microglia homeostatic state (Linnartz-Gerlach et al., 2014; Wang and Neumann, 2010). Additionally, we saw increased expression of microglial genes *CABLES1*, *TRIM14*, *MITF*, *MMP2*, and *SLC2A5*. Overall, these

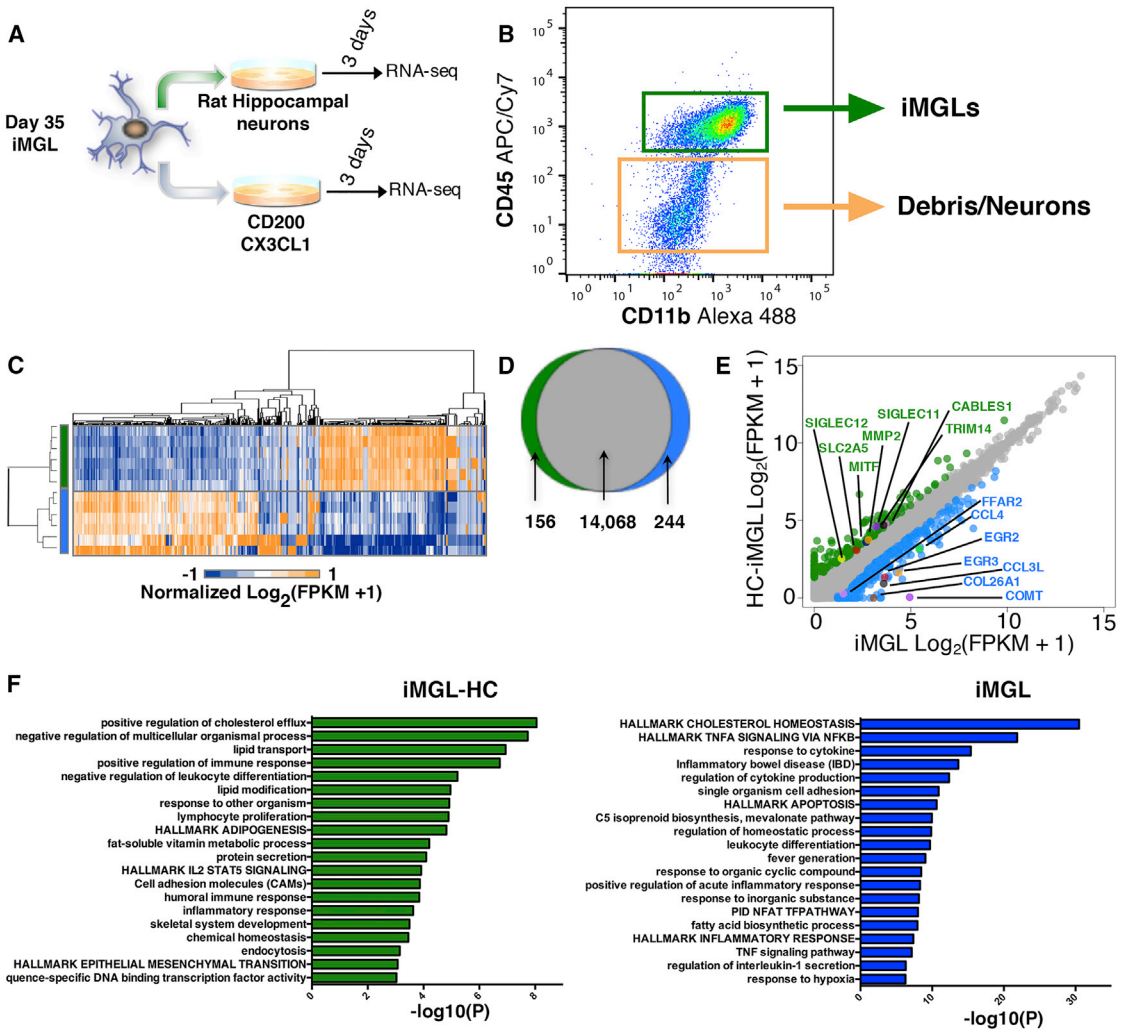

Figure 5. iMGLs Gene Profiles Are Responsive to Neuronal Environment

(A) Schematic of iMGL co-culture with or without rat hippocampal neurons.

(B) iMGLs co-cultured with neurons were collected and isolated by flow cytometry, and transcriptomes were evaluated via RNA sequencing.

(C) Heatmap of iMGLs and iMGL-HC gene expression highlights uniquely enriched genes.

(D) Differential gene expression analysis highlights 156 upregulated and 244 downregulated genes in iMGL-HCs.

(E) Scatterplot of differentially expressed genes, >2 [Log_2 (FPKM +1)], highlight *TRIM14*, *CABLES1*, *MMP2*, *SIGLEC11* and *SIGLEC12*, *MITF*, and *SLC2A5* being enriched in iMGL-HCs, suggesting that iMGLs respond appropriately to a neuronal environment. Cells cultured alone are enriched for *COMT*, *EGR2*, *EGR3*, and *FFAR2*, suggesting a primed microglia phenotype.

(F) GO and pathway terms from differential gene expression analysis of iMGLs cultured with hippocampal neurons. Genes upregulated in iMGL-HC are associated with 20 statistically significant pathway modules (green histogram), including positive cholesterol efflux, lipid transport, positive regulation of immune response, negative regulation of leukocyte differentiation, and cell adhesion molecules. Cells cultured in absence of neurons had a complimentary gene profile with 20 statistically significant biological modules (blue histogram), including hallmark cholesterol homeostasis, hallmark TNFα signaling via NF-κB, leukocyte differentiation, and regulation of IL-1β secretion.

results implicate both soluble and surface CNS cues as factors in microglia maturation (Biber et al., 2007) (Figures 5E and 5F).

A fundamental characteristic of microglia is the surveillance of the CNS environment with their highly ramified processes. To investigate how iMGLs might interact within a human brain environment and to test whether iMGLs invade BORGs similarly to how microglia enter the developing neural tube (Chan et al., 2007; Rezaie and Male, 1999), we cultured iMGLs with hiPSC 3D brain organoids (BORGs). BORGs include neurons, astrocytes, and oligodendrocytes that self-organize into a cortical-like network but lack microglia (Figure 6). By day 3, iMGLs had embedded into the BORGS and were not detected in the media, suggesting rapid iMGL chemotaxis toward CNS cues (Figures 6A–6C). By day 7, iMGLs (green) also tiled and extended varying degrees of ramified processes within the 3D organoid environment (Figures 6D–6F). To determine whether iMGLs respond to neuronal injury, we pierced BORGS with a 25G needle. After injury, iMGLs clustered near the injury site

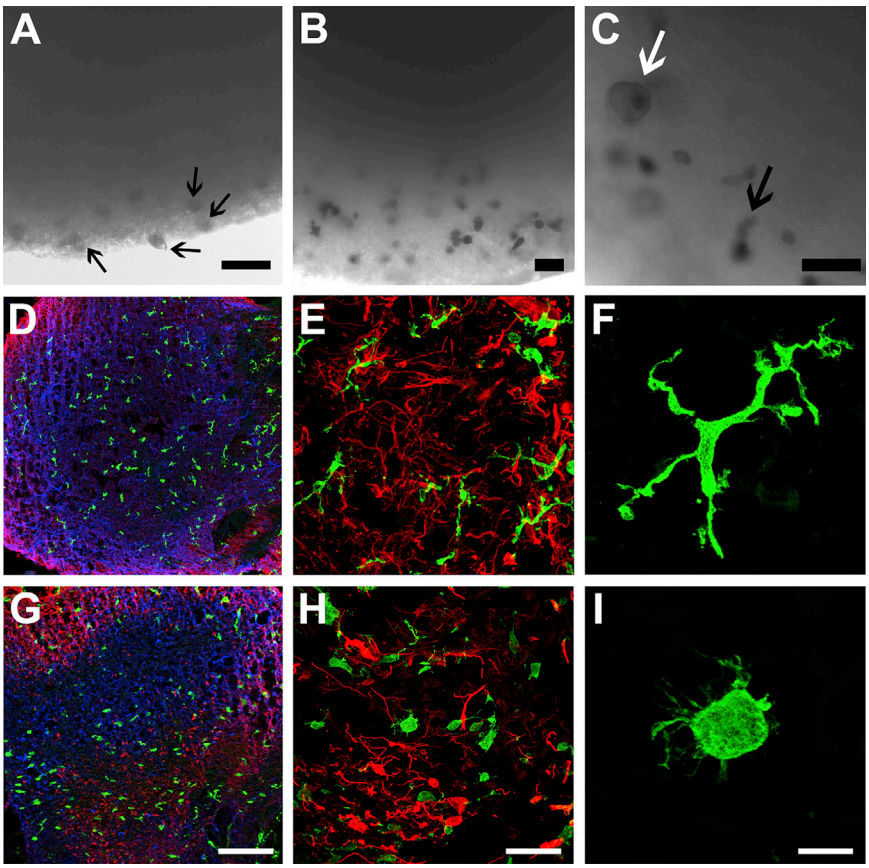

Figure 6. iMGLs Respond to the Neuronal Environment in 3D Brain Organoid Co-cultures

iMGLs (5×10^5 cells) were added to media containing a single brain organoid co-culture (BORG) for 7 days.

(A) Representative bright-field image of iMGLs detected in and near BORG after 3 days. iMGLs were found in and attached to the BORG-media interface (arrows), but not free floating in the media, suggesting complete chemotaxis of iMGLs.

(B) Representative image of iMGLs in outer and inner radius of BORG.

(C) Embedded iMGLs exhibit macrophage-like morphology (white arrow) and extend processes (arrow) signifying ECM remodeling and surveillance respectively.

(D–I) Simultaneous assessment of embedded iMGL morphology in uninjured (D–F) and injured (G–I) BORGs. Immunohistochemical analysis of BORGs reveals iMGLs begin tiling evenly throughout the BORG and project ramified processes for surveillance of the environment (D). BORGs are representative of developing brains in vitro and contain neurons (β3-tubulin, blue) and astrocytes (GFAP, red), which self-organize into a cortical-like distribution, but lack microglia. iMGLs (IBA1, green). Representative immunofluorescent images of iMGLs with extended processes within the 3D CNS environment at higher magnification (E and F). Representative images of iMGL morphology observed in injured BORG (G–I). Round-bodied iMGLs reminiscent of amoeboid microglia are distributed in injured BORGs and closely resemble activated microglia, demonstrating that iMGLs respond appropriately to neuronal injury (H and I). Scale bars, 50 μm in (A)–(C), 200 μm in (D) and (G), 80 μm in (E) and (H), and 15 μm in (F) and (I).

and adopted a more amoeboid morphology, resembling "activated" microglia found in injured or diseased brains (Kettenmann et al., 2011) (Figures 6G–6I). Collectively, these data demonstrate that iMGLs can integrate within an in vitro 3D CNS environment, mature, ramify, and respond to injury similar to brain microglia.

Next, we sought to examine iMGLs within the context of a CNS environment in vivo. To this end, we transplanted iMGLs (day 38) into the cortex of MITRG mice that are Rag2-deficient and IL2rγ-deficient mice and also express the human forms of four cytokines knocked in (M-CSF^h;IL-3/GM-CSF^h;TPO^h), allowing for xenotransplantation and survival of myeloid and other leukocytes (Rongvaux et al., 2014). 2 months after transplantation, the homeostatic state and identity of transplanted microglia were assessed with P2RY12 and the human-specific TMEM119 antibodies, respectively (Bennett et al., 2016; Butovsky et al., 2014; Haynes et al., 2006) (Figure 7). Human-specific markers, Ku80 (hNuclei) and cytoplasmic SC121 (hCyto), distinguished iMGLs from endogenous microglia. Transplanted human iMGLs co-expressing both Ku80 and P2RY12 were abundant within MITRG brains, suggesting long-term engraftment potential (Figures 7A–7D). At higher magnification, P2RY12 is expressed in highly ramified iMGLs resembling quiescent cortical microglia; the membrane distribution accentuates the finer extended processes (Figures 7B–7D) (Baron et al., 2014). TMEM119 and IBA1 were also expressed in both hCyto$^+$ soma and in highly arborized iMGL processes (Figures 7E–7L). At higher magnification, TMEM119 is predominately membrane bound, in agreement with previous studies (Bennett et al., 2016). Together, these findings demonstrate engraftment and long-term survival of iMGLs that result in highly branched, microglia-like cells expressing IBA1, P2RY12, and TMEM119 (Figures 7I–7L), in which iMGLs resemble endogenous quiescent microglia. Finally, the morphology and high P2RY12 expression suggest that transplanted iMGLs are actively surveying their neuronal environment that translates to their potential use in studying human microglia function in mouse CNS disease models.

To test this hypothesis, we transplanted iMGLs into the hippocampi of xenotransplantation-compatible AD mice, previously generated and characterized in our lab (Marsh et al., 2016), to examine how iMGLs interact with AD neuropathology in vivo (Figures 7M–7P; Figure S7). Transplanted iMGLs engraft and migrate along white matter tracts, similar to microglia in development (Figure 7M). In many instances, iMGLs migrated and extended processes toward Aβ plaques

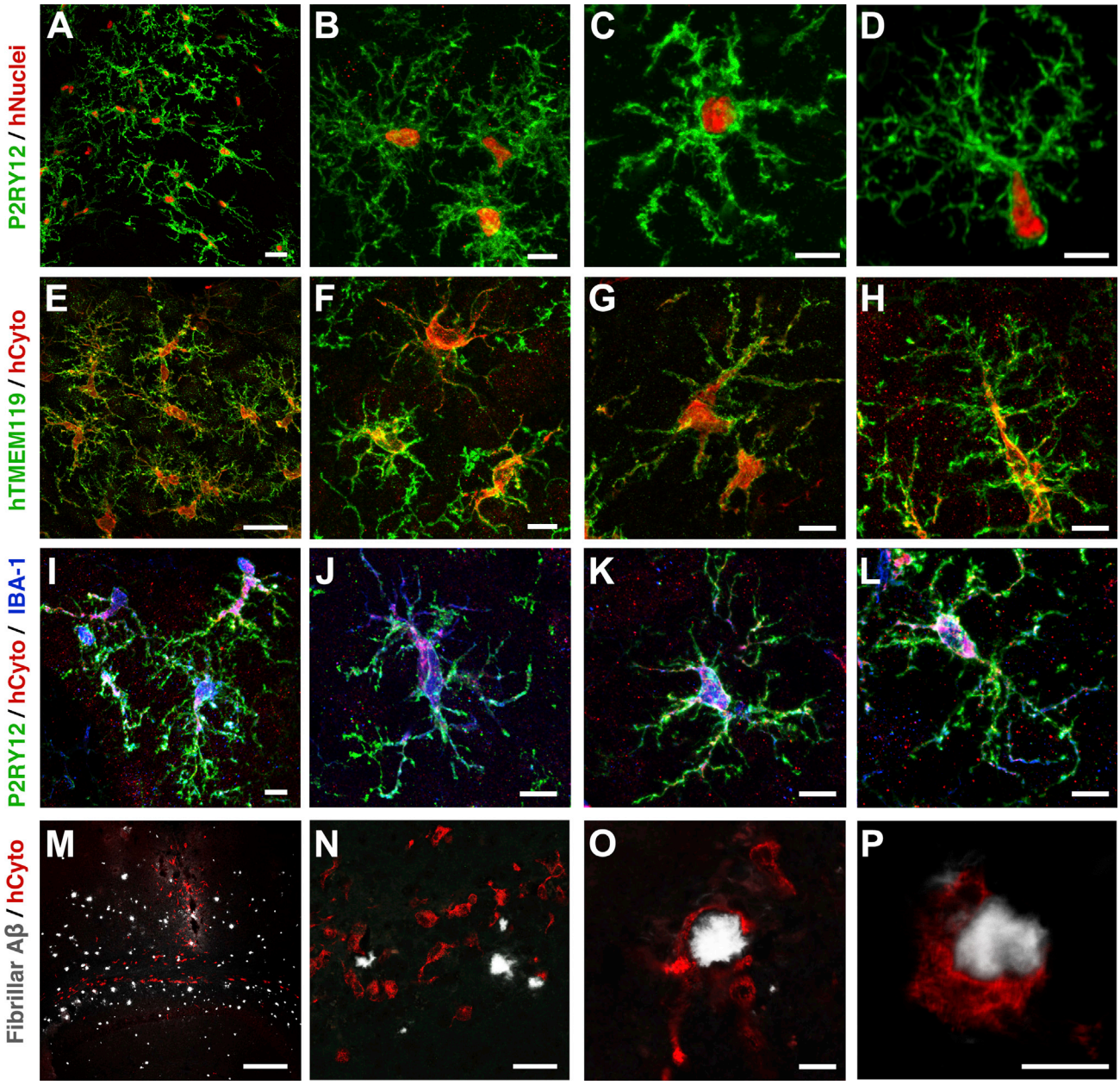

Figure 7. iMGLs Transplanted into the Brains of Either Wild-Type or AD Transplant Competent Mice Are Like Brain Microglia

Within the brains of xenotransplantation compatible mice, transplanted iMGLs are ramified and interact with the neuronal environment.

(A–L) After 2 months in vivo, iMGLs transplanted into mice display long-term viability with highly arborized processes resembling endogenous microglia found in the brain. Transplanted iMGLs, labeled with P2RY12 (green; HPA HPA014518, Sigma) and human nuclei (Ku80, red), exhibit long-term viability in mice (A). At higher magnification, P2RY12 is highly expressed in iMGL arborized processes, both suggestive of homeostatic microglia surveying the brain environment (B–D). Ramified iMGLs also express microglia-enriched TMEM119 recognized by a human-specific TMEM119 antibody (green; ab185333, Abcam, identified and validated in Bennett et al., 2016, and human cytoplasm maker SC121 (hCyto, red) (E–H). At higher magnification, representative iMGLs express P2RY12 (green), hCyto (red), and Iba1 (blue; ab5076, Abcam) (I–L).

(M–P) Human iMGLs (hCyto, red) transplanted into AD-immune-deficient mice (Marsh et al., 2016) interact with and phagocytose amyloid plaques (white). Transplanted iMGLs extend projections and migrate to plaques (M and N). iMGLs fully encompass amyloid plaques (O) and begin to phagocytose amyloid (P). Scale bars, 30 μm (A, E, and N), 10 μm (B–D, F–H, I–L, O, and P), and 300 μm (M). n = 3 animals per study. See also Figure S7.

to begin walling them off (Figures 7N–7P; Movie S1). A number of iMGLs also began to phagocytose fibrillar Aβ (Figures 7N–7P; Figures S7E–S7H). Similarly, human fetal microglia migrated toward Aβ, extended processes, and phagocytosed Aβ when transplanted in the same AD transgenic model (Figures S7A–S7D).

DISCUSSION

Here, we show that human microglia-like cells can be generated from iPSCs following a fully defined and highly efficient protocol, which enables high purity (>97%) and robust scalability. Importantly, iMGLs are highly similar to cultured human adult and fetal microglia by both transcriptomic and functional analyses. Our whole-transcriptome PCA also highlights the differentiation trajectory of iPSCs toward iHPCs and then iMGLs. Moreover, our series of microglial functional assays, only possible with a high yield and pure protocol, further strengthens how iMGLs can be used to investigate microglia genes implicated in disease and understand physiological function both in vitro and in vivo.

We also demonstrate the use of iMGLs to investigate human microglial function as a therapeutic target in human disease. A recent study implicated complement and increased microglia-mediated pruning of synapses early in AD (Hong et al., 2016a, 2016b). Here, we found that blocking CR3, via anti-CD11b, in iMGLs reduced phagocytosis of human synaptosomes. Our findings provide one of the first examples, to our knowledge, of quantitative evidence showing human microglia engulfing human synaptosomes predominately via the CR3 axis, as implicated by transgenic mouse studies (Hong et al., 2016a). Moreover, we highlight the utility of iMGLs to examine microglia-targeted AD therapies, such as anti-CD11b, in phagocytic assays and to potentially examine or validate other complement-targeted therapies in development.

Microglia mediate neuroinflammation through surveillance of their environment and by cell surface receptor activation. Therefore, we tested iMGL response to extracellular stimuli observed in AD, such as nucleotides leaked from degenerating neurons. Microglia sense ADP release via purinergic receptors, and we likewise find that iMGLs robustly express functional P2RY12 and migrate and exhibit calcium influx via an ADP-P2RY12 receptor mechanism. Also, iMGLs secrete a variety of cytokines in response to IFNγ, IL-1β, and LPS stimulation. Many of these cytokines are known to be highly elevated in neurological diseases and/or involved in the recruitment of peripheral immune cells into the CNS under pathological conditions (Chan et al., 2007; Prinz et al., 2011; Rezaie and Male, 1999; Stalder et al., 2005). Microglial-mediated cytokine secretion can further influence the inflammatory milieu in the CNS and thus represents an excellent therapeutic target for restoring CNS homeostatic balance. Together, migration, calcium imaging, and cytokine secretion assays not only validate iMGLs to be highly similar to brain-derived microglia, but provide important functional assays to assess the role of microglia in neuroinflammation. Furthermore, our data highlight the potential utility of iMGLs to identify therapeutic compounds via high-throughput assessment of microglia physiology.

Since the discovery of SNPs in immune genes as AD risk factors, microglia have been further highlighted in human neurological health and disease. Several of these AD-GWAS genes, including *CD33* and *CR1*, lack functionally similar murine orthologs. Thus, iMGLs can be utilized to investigate AD-GWAS genes and elucidate their roles in human microglia biology. Aβ fibrils upregulated *APOE*, *TREM2*, *CD33*, and *APOJ*, genes previously implicated in modulating Aβ phagocytosis and clearance (Bradshaw et al., 2013; Yeh et al., 2016). We also found that *MS4A6A* gene expression was increased. While the role of the MS4A gene cluster in microglia function and AD risk is still unknown, our data suggest a potential role in modulating Aβ interactions. Furthermore, CD200 and CX3CL1 were important developmental CNS cues for generating iMGLs that can respond appropriately to Aβ. These data implicate these factors in modulating promoter/enhancer regions that enables appropriate responses to stimuli previously shown for macrophages (Gosselin et al., 2014; Lavin et al., 2014) (further reviewed in Glass and Natoli, 2016). Lastly, a TGFβ-dependent homeostatic microglia signature was identified that paralleled murine studies and highlight that AD-GWAS genes function in microglia homeostasis. Taken together, our studies emphasize the importance of microglia in AD risk and the utility of iMGLs to interrogate genotype-phenotype relationships of recent AD-GWAS single nucleotide polymorphisms.

We also highlight how neuronal co-culture can further modulate microglial gene expression and how interactions with the neuronal glycocalyx increase Siglec expression. Interestingly, iMGLs not cultured with neurons differentially expressed early microglia genes, including *FFAR2* (Erny et al., 2015; Matcovitch-Natan et al., 2016), suggesting that other factors are needed to further educate microglia as tissue-resident macrophages of the brain. In accordance with this notion, iMGLs cultured in 3D brain cultures actively migrate, tile, and encompass the volume of the BORGs, extending processes reminiscent of early microglia development. We also show that iMGLs transplanted in mice, engraft, survive, and display characteristic ramified processes that have increased branch order complexity, closely resembling quiescent microglia (Andreasson et al., 2016). We also note that transplanted, highly ramified iMGLs were morphological heterogeneous within the brain (Figures 7I–7L). This morphological diversity is indicative of microglia responding to distinct cortical layers/brain regions and potentially reflect microglia subtypes found within the brain (Grabert et al., 2016). Our results also demonstrate that iMGLs can respond appropriately to the neurotoxic buildup of Aβ, thus providing a model system to investigate the role of microglia in various proteinopathies.

Overall, these results underscore the potential of iMGLs as a renewable source of patient-derived, microglial-like cells for studying the role of microglia in neurodegenerative diseases. While our comparisons were limited to cultured microglia, we showed that our cells were highly similar to primary cells, and our studies have highlighted potential new ways to culture microglia within BORGs or mouse brains. For example, transplantation of iMGLs into various CNS disease mouse models will allow for the study of human microglial function in neurodegenerative disease in vivo that may be influenced by genetics and the inheritance of specific mutations. This platform will allow for the identification of potential novel, microglial-based translational therapies, as recently discussed (Biber et al., 2016). Finally, while technical challenges exist for isolating microglia from both human brain and BORGS for study, the development of future tools will likely make it feasible to compare microglia isolated from BORGs with freshly isolated microglia to determine whether 3D organoid systems fully recapitulate the in vivo microglia signature. In summary, we demonstrate a methodology to generate human

microglial-like cells in large quantities from renewable iPSCs that can be used as primary microglia surrogates.

Our study is one of the first to describe a fully defined, serum-free protocol for generating microglial cells from induced pluripotent stem cells with the exception of a recently published resource from Muffat and colleagues (Muffat et al., 2016). However, their approach uses hematopoietic cells derived from embryoid bodies (EBs) as microglia precursors. One challenge with the use of an EB-based method and selection by cell adhesion (Muffat et al. 2016 protocol) is the potential contamination by other cell types that spontaneously arise from EBs, i.e., neuroectoderm including astrocytes. More recently, a protocol described the production of microglia-like cells reliant on astrocyte co-cultures and a serum-based media formulation. This protocol produces cell quantities comparable to Muffat et al. (2016) that exhibit amoeboid-like morphology in vitro and in vivo (Pandya et al., 2017). Thus, some questions remain in terms of yield, scalability, and purity of homeostatic microglia using these other methods and whether the resulting cells can be used to interrogate microglial function in quantitative assays that require large numbers of pure microglia-like cells.

In summary, we have developed a highly reproducible protocol to generate iPSC-derived hematopoietic progenitor cells and microglia-like cells in high yield that can be used in functional assays to interrogate microglia function. We have also identified a commercial HPC source that can be readily differentiated to iMGLs with our protocol to study microglia biology. We demonstrate that iMGLs phagocytose a variety of neuronal substrates, including β-amyloid, brain-derived tau oligomers, and human synaptosomes, that can be used to study the influence of AD genetic risk factors, including recently identified novel *TREM2* variants (Sirkis et al., 2016) on microglia function, with the potential to uncover altered microglia pathways that can guide future therapeutic targets. Because many AD-GWAS genes also suggest microglia-neuronal crosstalk (e.g., *TREM2*-lipids, *APOE/J*, *CD33*-sialic acid, *MS4A* cluster/lipids), we demonstrated that iMGLs can be studied in context with neurons and glia by examining how both rodent and human neuronal cells influence microglia phenotype and function both in vitro and in vivo. As expected, iMGLs gene profiles shift toward a neuronal-centric phenotype and respond appropriately to injury in 3D cell culture and β-amyloid plaques in AD transgenic mice brains. Together, our fully defined protocol yields highly pure microglia-like cells that provide a platform to investigate human microglia function for a broad range of CNS development, homeostatic function, and neurological disease applications. While the validation of iMGLs as microglia surrogates raised several new and exciting questions related to microglia biology in development, health, and disease, this new renewable resource will allow for those questions to be further addressed by the field.

STAR★METHODS

Detailed methods are provided in the online version of this paper and include the following:

- KEY RESOURCE TABLE
- CONTACT FOR REAGENT AND RESOURCE SHARING
- EXPERIMENTAL MODEL AND SUBJECT DETAILS
  - Chemical Reagents
  - Cell Culture
- METHOD DETAILS
  - RNA-Seq Library Construction
  - Confocal Microscopy and Bright-Field Imaging
  - FACS and Flow Cytometer Analysis
  - Cytospin and May-Grunwald Giemsa Stain
  - RNA Isolation and qPCR Analysis
  - iMGL Co-culture with Rat Neurons
  - iMGL Transplantation in MITRG and Rag-5xfAD Brains
  - Immunocytochemistry and Immunohistochemistry
  - ADP Migration and Calcium Imaging Assays
  - Phagocytosis Assays
  - Fibrillar Aβ Preparation
  - BDTO Preparation
  - Human Synaptosomes
  - Mesoscale Multiplex Cytokine and Chemokine Assay
  - Dot Blot
  - AD-GWAS qPCR Primers
- QUANTIFICATION AND STATISTICAL ANALYSIS
  - RNA-Seq Analysis
  - Statistical Analysis
- DATA AND SOFTWARE AVAILABILITY

SUPPLEMENTAL INFORMATION

Supplemental Information includes seven figures, seven tables, and one movie and can be found with this article online at http://dx.doi.org/10.1016/j.neuron.2017.03.042.

AUTHOR CONTRIBUTIONS

E.M.A. and M.B.-J. conceived the project. E.M.A., R.N.R., E.S.M., M.J.C., W.W.P., and M.B.-J. designed and supervised experiments and interpreted results. E.M.A. and E.S.M. designed the differentiation method and growth of iHPCs. E.M.A. designed the differentiation method and growth of iMGLs. A.A. provided DC RNA. L.M.H. and J.P.A. provided fetal and adult microglia RNA. R.N.R., E.M.A., and W.W.P. designed and performed transcriptome analysis with input from A.M. E.M.A., E.S.M., and W.W.P. designed, performed, and analyzed functional assays. S.A.N. and B.J.C. developed the 3D BORGs. E.M.A. and A.V.Y. designed, performed, and analyzed calcium imaging with input from M.D.C. E.M.A. and V.S.M. designed, performed, and analyzed flow cytometer studies. E.M.A., S.E.M., and G.M.F. performed transplantation studies. E.M.A., M.B.J., and S.E.M. performed immunofluorescence imaging analysis. A.M.M. generated preliminary data. K.H.G. isolated and C.F. prepared, processed, and labeled synaptosomes. C.A.C. prepared neuronal cultures. R.K. isolated and characterized BDTOs, and C.F. processed and labeled BDTOs. E.M.A. and W.W.P. performed all other experiments and analysis. C.H.H.N. and G.M.F. assisted with cell culture, sample prep, and data analysis. E.M.A., R.N.R., E.S.M., W.W.P., and M.B.-J. wrote the paper, and all authors provided feedback.

ACKNOWLEDGMENTS

This work was supported by NIH AG048099 (M.B.-J.), AG016573 (M.B.-J. and W.W.P.), AG054025 (R.K.), CIRM RT3-07893 (M.B.-J.), Alzheimer's Association BFG-14-317000 (M.B.-J.), a Stem Cell Research Center SEED grant for BORGs (B.J.C.), UC Irvine MSTP NIH T32-GM008620 (E.M.A. and G.M.F.), a Burden Fellowship (A.M.M.), and a generous gift from the Susan Scott Foundation (M.B.-J.). iPSC lines were generated by the UCI-ADRC iPS cell core funded by NIH AG016573. We thank the UCI High-Throughput Genomics Core, the Institute for Immunology, and Dr. Jennifer Atwood and Dr. Melanie

Oakes. Blood donor program was supported by the NCRR and the NCATS through Grant UL1 TR001414. The content is solely the responsibility of the authors and does not necessarily represent the official views of the NIH.

Received: October 25, 2016
Revised: February 16, 2017
Accepted: March 28, 2017
Published: April 19, 2017

REFERENCES

Abbas, N., Bednar, I., Mix, E., Marie, S., Paterson, D., Ljungberg, A., Morris, C., Winblad, B., Nordberg, A., and Zhu, J. (2002). Up-regulation of the inflammatory cytokines IFN-gamma and IL-12 and down-regulation of IL-4 in cerebral cortex regions of APP(SWE) transgenic mice. J. Neuroimmunol. *126*, 50–57.

Abdollahi, A., Lord, K.A., Hoffman-Liebermann, B., and Liebermann, D.A. (1991). Interferon regulatory factor 1 is a myeloid differentiation primary response gene induced by interleukin 6 and leukemia inhibitory factor: role in growth inhibition. Cell Growth Differ. *2*, 401–407.

Abutbul, S., Shapiro, J., Szaingurten-Solodkin, I., Levy, N., Carmy, Y., Baron, R., Jung, S., and Monsonego, A. (2012). TGF-β signaling through SMAD2/3 induces the quiescent microglial phenotype within the CNS environment. Glia *60*, 1160–1171.

Aguzzi, A., Barres, B.A., and Bennett, M.L. (2013). Microglia: scapegoat, saboteur, or something else? Science *339*, 156–161.

Andreasson, K.I., Bachstetter, A.D., Colonna, M., Ginhoux, F., Holmes, C., Lamb, B., Landreth, G., Lee, D.C., Low, D., Lynch, M.A., et al. (2016). Targeting innate immunity for neurodegenerative disorders of the central nervous system. J. Neurochem. *138*, 653–693.

Asai, H., Ikezu, S., Tsunoda, S., Medalla, M., Luebke, J., Haydar, T., Wolozin, B., Butovsky, O., Kügler, S., and Ikezu, T. (2015). Depletion of microglia and inhibition of exosome synthesis halt tau propagation. Nat. Neurosci. *18*, 1584–1593.

Bachstetter, A.D., Van Eldik, L.J., Schmitt, F.A., Neltner, J.H., Ighodaro, E.T., Webster, S.J., Patel, E., Abner, E.L., Kryscio, R.J., and Nelson, P.T. (2015). Disease-related microglia heterogeneity in the hippocampus of Alzheimer's disease, dementia with Lewy bodies, and hippocampal sclerosis of aging. Acta Neuropathol. Commun. *3*, 32.

Baron, R., Babcock, A.A., Nemirovsky, A., Finsen, B., and Monsonego, A. (2014). Accelerated microglial pathology is associated with Aβ plaques in mouse models of Alzheimer's disease. Aging Cell *13*, 584–595.

Bennett, M.L., Bennett, F.C., Liddelow, S.A., Ajami, B., Zamanian, J.L., Fernhoff, N.B., Mulinyawe, S.B., Bohlen, C.J., Adil, A., Tucker, A., et al. (2016). New tools for studying microglia in the mouse and human CNS. Proc. Natl. Acad. Sci. USA *113*, E1738–E1746.

Biber, K., Neumann, H., Inoue, K., and Boddeke, H.W. (2007). Neuronal 'On' and 'Off' signals control microglia. Trends Neurosci. *30*, 596–602.

Biber, K., Möller, T., Boddeke, E., and Prinz, M. (2016). Central nervous system myeloid cells as drug targets: current status and translational challenges. Nat. Rev. Drug Discov. *15*, 110–124.

Blum-Degen, D., Müller, T., Kuhn, W., Gerlach, M., Przuntek, H., and Riederer, P. (1995). Interleukin-1 beta and interleukin-6 are elevated in the cerebrospinal fluid of Alzheimer's and de novo Parkinson's disease patients. Neurosci. Lett. *202*, 17–20.

Blurton-Jones, M., Kitazawa, M., Martinez-Coria, H., Castello, N.A., Müller, F.J., Loring, J.F., Yamasaki, T.R., Poon, W.W., Green, K.N., and LaFerla, F.M. (2009). Neural stem cells improve cognition via BDNF in a transgenic model of Alzheimer disease. Proc. Natl. Acad. Sci. U.S.A. *106*, 13594–13599.

Bradshaw, E.M., Chibnik, L.B., Keenan, B.T., Ottoboni, L., Raj, T., Tang, A., Rosenkrantz, L.L., Imboywa, S., Lee, M., Von Korff, A., et al.; Alzheimer Disease Neuroimaging Initiative (2013). CD33 Alzheimer's disease locus: altered monocyte function and amyloid biology. Nat. Neurosci. *16*, 848–850.

Butovsky, O., Jedrychowski, M.P., Moore, C.S., Cialic, R., Lanser, A.J., Gabriely, G., Koeglsperger, T., Dake, B., Wu, P.M., Doykan, C.E., et al. (2014). Identification of a unique TGF-β-dependent molecular and functional signature in microglia. Nat. Neurosci. *17*, 131–143.

Chan, W.Y., Kohsaka, S., and Rezaie, P. (2007). The origin and cell lineage of microglia: new concepts. Brain Res. Brain Res. Rev. *53*, 344–354.

Chen, E.Y., Tan, C.M., Kou, Y., Duan, Q., Wang, Z., Meirelles, G.V., Clark, N.R., and Ma'ayan, A. (2013). Enrichr: interactive and collaborative HTML5 gene list enrichment analysis tool. BMC Bioinformatics *14*, 128.

Chung, W.S., Clarke, L.E., Wang, G.X., Stafford, B.K., Sher, A., Chakraborty, C., Joung, J., Foo, L.C., Thompson, A., Chen, C., et al. (2013). Astrocytes mediate synapse elimination through MEGF10 and MERTK pathways. Nature *504*, 394–400.

Crotti, A., Benner, C., Kerman, B.E., Gosselin, D., Lagier-Tourenne, C., Zuccato, C., Cattaneo, E., Gage, F.H., Cleveland, D.W., and Glass, C.K. (2014). Mutant Huntingtin promotes autonomous microglia activation via myeloid lineage-determining factors. Nat. Neurosci. *17*, 513–521.

De Simone, R., Niturad, C.E., De Nuccio, C., Ajmone-Cat, M.A., Visentin, S., and Minghetti, L. (2010). TGF-β and LPS modulate ADP-induced migration of microglial cells through P2Y1 and P2Y12 receptor expression. J. Neurochem. *115*, 450–459.

Dobin, A., Davis, C.A., Schlesinger, F., Drenkow, J., Zaleski, C., Jha, S., Batut, P., Chaisson, M., and Gingeras, T.R. (2013). STAR: ultrafast universal RNA-seq aligner. Bioinformatics *29*, 15–21.

Durafourt, B.A., Moore, C.S., Blain, M., and Antel, J.P. (2013). Isolating, culturing, and polarizing primary human adult and fetal microglia. Methods Mol. Biol. *1041*, 199–211.

Erny, D., Hrabě de Angelis, A.L., Jaitin, D., Wieghofer, P., Staszewski, O., David, E., Keren-Shaul, H., Mahlakoiv, T., Jakobshagen, K., Buch, T., et al. (2015). Host microbiota constantly control maturation and function of microglia in the CNS. Nat. Neurosci. *18*, 965–977.

Fu, Y., Hsiao, J.H., Paxinos, G., Halliday, G.M., and Kim, W.S. (2016). ABCA7 mediates phagocytic clearance of amyloid-β in the brain. J. Alzheimers Dis. *54*, 569–584.

Ginhoux, F., Greter, M., Leboeuf, M., Nandi, S., See, P., Gokhan, S., Mehler, M.F., Conway, S.J., Ng, L.G., Stanley, E.R., et al. (2010). Fate mapping analysis reveals that adult microglia derive from primitive macrophages. Science *330*, 841–845.

Glass, C.K., and Natoli, G. (2016). Molecular control of activation and priming in macrophages. Nat. Immunol. *17*, 26–33.

Gosselin, D., Link, V.M., Romanoski, C.E., Fonseca, G.J., Eichenfield, D.Z., Spann, N.J., Stender, J.D., Chun, H.B., Garner, H., Geissmann, F., and Glass, C.K. (2014). Environment drives selection and function of enhancers controlling tissue-specific macrophage identities. Cell *159*, 1327–1340.

Grabert, K., Michoel, T., Karavolos, M.H., Clohisey, S., Baillie, J.K., Stevens, M.P., Freeman, T.C., Summers, K.M., and McColl, B.W. (2016). Microglial brain region-dependent diversity and selective regional sensitivities to aging. Nat. Neurosci. *19*, 504–516.

Greer, P.L., Bear, D.M., Lassance, J.M., Bloom, M.L., Tsukahara, T., Pashkovski, S.L., Masuda, F.K., Nowlan, A.C., Kirchner, R., Hoekstra, H.E., and Datta, S.R. (2016). A family of non-GPCR chemosensors defines an alternative logic for mammalian olfaction. Cell *165*, 1734–1748.

Greter, M., Lelios, I., Pelczar, P., Hoeffel, G., Price, J., Leboeuf, M., Kündig, T.M., Frei, K., Ginhoux, F., Merad, M., and Becher, B. (2012). Stroma-derived interleukin-34 controls the development and maintenance of langerhans cells and the maintenance of microglia. Immunity *37*, 1050–1060.

Guillot-Sestier, M.V., and Town, T. (2013). Innate immunity in Alzheimer's disease: a complex affair. CNS Neurol. Disord. Drug Targets *12*, 593–607.

Gylys, K.H., Fein, J.A., and Cole, G.M. (2000). Quantitative characterization of crude synaptosomal fraction (P-2) components by flow cytometry. J. Neurosci. Res. *61*, 186–192.

Hanna, R.N., Carlin, L.M., Hubbeling, H.G., Nackiewicz, D., Green, A.M., Punt, J.A., Geissmann, F., and Hedrick, C.C. (2011). The transcription factor NR4A1 (Nur77) controls bone marrow differentiation and the survival of Ly6C- monocytes. Nat. Immunol. *12*, 778–785.

Haynes, S.E., Hollopeter, G., Yang, G., Kurpius, D., Dailey, M.E., Gan, W.B., and Julius, D. (2006). The P2Y12 receptor regulates microglial activation by extracellular nucleotides. Nat. Neurosci. *9*, 1512–1519.

Hickman, S.E., Allison, E.K., and El Khoury, J. (2008). Microglial dysfunction and defective beta-amyloid clearance pathways in aging Alzheimer's disease mice. J. Neurosci. *28*, 8354–8360.

Hickman, S.E., Kingery, N.D., Ohsumi, T.K., Borowsky, M.L., Wang, L.C., Means, T.K., and El Khoury, J. (2013). The microglial sensome revealed by direct RNA sequencing. Nat. Neurosci. *16*, 1896–1905.

Hong, S., Beja-Glasser, V.F., Nfonoyim, B.M., Frouin, A., Li, S., Ramakrishnan, S., Merry, K.M., Shi, Q., Rosenthal, A., Barres, B.A., et al. (2016a). Complement and microglia mediate early synapse loss in Alzheimer mouse models. Science *352*, 712–716.

Hong, S., Dissing-Olesen, L., and Stevens, B. (2016b). New insights on the role of microglia in synaptic pruning in health and disease. Curr. Opin. Neurobiol. *36*, 128–134.

Karch, C.M., Ezerskiy, L.A., Bertelsen, S., and Goate, A.M.; Alzheimer's Disease Genetics Consortium (ADGC) (2016). Alzheimer's disease risk polymorphisms regulate gene expression in the ZCWPW1 and the CELF1 loci. PLoS ONE *11*, e0148717.

Kennedy, M., D'Souza, S.L., Lynch-Kattman, M., Schwantz, S., and Keller, G. (2007). Development of the hemangioblast defines the onset of hematopoiesis in human ES cell differentiation cultures. Blood *109*, 2679–2687.

Kettenmann, H., Hanisch, U.K., Noda, M., and Verkhratsky, A. (2011). Physiology of microglia. Physiol. Rev. *91*, 461–553.

Kierdorf, K., and Prinz, M. (2013). Factors regulating microglia activation. Front. Cell. Neurosci. *7*, 44.

Kierdorf, K., Erny, D., Goldmann, T., Sander, V., Schulz, C., Perdiguero, E.G., Wieghofer, P., Heinrich, A., Riemke, P., Hölscher, C., et al. (2013). Microglia emerge from erythromyeloid precursors via Pu.1- and Irf8-dependent pathways. Nat. Neurosci. *16*, 273–280.

Koenigsknecht-Talboo, J., and Landreth, G.E. (2005). Microglial phagocytosis induced by fibrillar beta-amyloid and IgGs are differentially regulated by proinflammatory cytokines. J. Neurosci. *25*, 8240–8249.

Kuleshov, M.V., Jones, M.R., Rouillard, A.D., Fernandez, N.F., Duan, Q., Wang, Z., Koplev, S., Jenkins, S.L., Jagodnik, K.M., Lachmann, A., et al. (2016). Enrichr: a comprehensive gene set enrichment analysis web server 2016 update. Nucleic Acids Res. *44* (W1), W90-7.

Lancaster, M.A., Renner, M., Martin, C.A., Wenzel, D., Bicknell, L.S., Hurles, M.E., Homfray, T., Penninger, J.M., Jackson, A.P., and Knoblich, J.A. (2013). Cerebral organoids model human brain development and microcephaly. Nature *501*, 373–379.

Lasagna-Reeves, C.A., Castillo-Carranza, D.L., Sengupta, U., Sarmiento, J., Troncoso, J., Jackson, G.R., and Kayed, R. (2012). Identification of oligomers at early stages of tau aggregation in Alzheimer's disease. FASEB J. *26*, 1946–1959.

Lavin, Y., Winter, D., Blecher-Gonen, R., David, E., Keren-Shaul, H., Merad, M., Jung, S., and Amit, I. (2014). Tissue-resident macrophage enhancer landscapes are shaped by the local microenvironment. Cell *159*, 1312–1326.

Li, B., and Dewey, C.N. (2011). RSEM: accurate transcript quantification from RNA-seq data with or without a reference genome. BMC Bioinformatics *12*, 323.

Linnartz-Gerlach, B., Mathews, M., and Neumann, H. (2014). Sensing the neuronal glycocalyx by glial sialic acid binding immunoglobulin-like lectins. Neuroscience *275*, 113–124.

Liu, Z., Condello, C., Schain, A., Harb, R., and Grutzendler, J. (2010). CX3CR1 in microglia regulates brain amyloid deposition through selective protofibrillar amyloid-β phagocytosis. J. Neurosci. *30*, 17091–17101.

Loo, D.T., Copani, A., Pike, C.J., Whittemore, E.R., Walencewicz, A.J., and Cotman, C.W. (1993). Apoptosis is induced by beta-amyloid in cultured central nervous system neurons. Proc. Natl. Acad. Sci. USA *90*, 7951–7955.

Lui, H., Zhang, J., Makinson, S.R., Cahill, M.K., Kelley, K.W., Huang, H.Y., Shang, Y., Oldham, M.C., Martens, L.H., Gao, F., et al. (2016). Progranulin deficiency promotes circuit-specific synaptic pruning by microglia via complement activation. Cell *165*, 921–935.

Marsh, S.E., Abud, E.M., Lakatos, A., Karimzadeh, A., Yeung, S.T., Davtyan, H., Fote, G.M., Lau, L., Weinger, J.G., Lane, T.E., et al. (2016). The adaptive immune system restrains Alzheimer's disease pathogenesis by modulating microglial function. Proc. Natl. Acad. Sci. USA *113*, E1316–E1325.

Matcovitch-Natan, O., Winter, D.R., Giladi, A., Vargas Aguilar, S., Spinrad, A., Sarrazin, S., Ben-Yehuda, H., David, E., Zelada González, F., Perrin, P., et al. (2016). Microglia development follows a stepwise program to regulate brain homeostasis. Science *353*, aad8670.

Moore, C.S., Ase, A.R., Kinsara, A., Rao, V.T., Michell-Robinson, M., Leong, S.Y., Butovsky, O., Ludwin, S.K., Séguéla, P., Bar-Or, A., and Antel, J.P. (2015). P2Y12 expression and function in alternatively activated human microglia. Neurol. Neuroimmunol. Neuroinflamm. *2*, e80.

Muffat, J., Li, Y., Yuan, B., Mitalipova, M., Omer, A., Corcoran, S., Bakiasi, G., Tsai, L.H., Aubourg, P., Ransohoff, R.M., and Jaenisch, R. (2016). Efficient derivation of microglia-like cells from human pluripotent stem cells. Nat. Med. *22*, 1358–1367.

O'Rourke, J.G., Bogdanik, L., Yáñez, A., Lall, D., Wolf, A.J., Muhammad, A.K., Ho, R., Carmona, S., Vit, J.P., Zarrow, J., et al. (2016). C9orf72 is required for proper macrophage and microglial function in mice. Science *351*, 1324–1329.

Pandya, H., Shen, M.J., Ichikawa, D.M., Sedlock, A.B., Choi, Y., Johnson, K.R., Kim, G., Brown, M.A., Elkahloun, A.G., Maric, D., et al. (2017). Differentiation of human and murine induced pluripotent stem cells to microglia-like cells. Nat. Neurosci. Published online March 2, 2017. http://dx.doi.org/10.1038/nn.4534.

Paolicelli, R.C., Bolasco, G., Pagani, F., Maggi, L., Scianni, M., Panzanelli, P., Giustetto, M., Ferreira, T.A., Guiducci, E., Dumas, L., et al. (2011). Synaptic pruning by microglia is necessary for normal brain development. Science *333*, 1456–1458.

Patel, N.S., Paris, D., Mathura, V., Quadros, A.N., Crawford, F.C., and Mullan, M.J. (2005). Inflammatory cytokine levels correlate with amyloid load in transgenic mouse models of Alzheimer's disease. J. Neuroinflammation *2*, 9.

Prinz, M., and Priller, J. (2014). Microglia and brain macrophages in the molecular age: from origin to neuropsychiatric disease. Nat. Rev. Neurosci. *15*, 300–312.

Prinz, M., Priller, J., Sisodia, S.S., and Ransohoff, R.M. (2011). Heterogeneity of CNS myeloid cells and their roles in neurodegeneration. Nat. Neurosci. *14*, 1227–1235.

Rezaie, P., and Male, D. (1999). Colonisation of the developing human brain and spinal cord by microglia: a review. Microsc. Res. Tech. *45*, 359–382.

Robinson, M.D., McCarthy, D.J., and Smyth, G.K. (2010). edgeR: a Bioconductor package for differential expression analysis of digital gene expression data. Bioinformatics *26*, 139–140.

Rongvaux, A., Willinger, T., Martinek, J., Strowig, T., Gearty, S.V., Teichmann, L.L., Saito, Y., Marches, F., Halene, S., Palucka, A.K., et al. (2014). Development and function of human innate immune cells in a humanized mouse model. Nat. Biotechnol. *32*, 364–372.

Rustenhoven, J., Park, T.I., Schweder, P., Scotter, J., Correia, J., Smith, A.M., Gibbons, H.M., Oldfield, R.L., Bergin, P.S., Mee, E.W., et al. (2016). Isolation of highly enriched primary human microglia for functional studies. Sci. Rep. *6*, 19371.

Schilling, T., Nitsch, R., Heinemann, U., Haas, D., and Eder, C. (2001). Astrocyte-released cytokines induce ramification and outward K+ channel expression in microglia via distinct signalling pathways. Eur. J. Neurosci. *14*, 463–473.

Schulz, C., Gomez Perdiguero, E., Chorro, L., Szabo-Rogers, H., Cagnard, N., Kierdorf, K., Prinz, M., Wu, B., Jacobsen, S.E., Pollard, J.W., et al. (2012). A lineage of myeloid cells independent of Myb and hematopoietic stem cells. Science *336*, 86–90.

Shulman, J.M., Imboywa, S., Giagtzoglou, N., Powers, M.P., Hu, Y., Devenport, D., Chipendo, P., Chibnik, L.B., Diamond, A., Perrimon, N., et al. (2014). Functional screening in Drosophila identifies Alzheimer's disease

susceptibility genes and implicates Tau-mediated mechanisms. Hum. Mol. Genet. *23*, 870–877.

Sirkis, D.W., Bonham, L.W., Aparicio, R.E., Geier, E.G., Ramos, E.M., Wang, Q., Karydas, A., Miller, Z.A., Miller, B.L., Coppola, G., and Yokoyama, J.S. (2016). Rare TREM2 variants associated with Alzheimer's disease display reduced cell surface expression. Acta Neuropathol. Commun. *4*, 98.

Stalder, A.K., Ermini, F., Bondolfi, L., Krenger, W., Burbach, G.J., Deller, T., Coomaraswamy, J., Staufenbiel, M., Landmann, R., and Jucker, M. (2005). Invasion of hematopoietic cells into the brain of amyloid precursor protein transgenic mice. J. Neurosci. *25*, 11125–11132.

Stephan, A.H., Barres, B.A., and Stevens, B. (2012). The complement system: an unexpected role in synaptic pruning during development and disease. Annu. Rev. Neurosci. *35*, 369–389.

Sturgeon, C.M., Ditadi, A., Awong, G., Kennedy, M., and Keller, G. (2014). Wnt signaling controls the specification of definitive and primitive hematopoiesis from human pluripotent stem cells. Nat. Biotechnol. *32*, 554–561.

Villegas-Llerena, C., Phillips, A., Garcia-Reitboeck, P., Hardy, J., and Pocock, J.M. (2016). Microglial genes regulating neuroinflammation in the progression of Alzheimer's disease. Curr. Opin. Neurobiol. *36*, 74–81.

Wang, Y., and Neumann, H. (2010). Alleviation of neurotoxicity by microglial human Siglec-11. J. Neurosci. *30*, 3482–3488.

Wang, Y., Szretter, K.J., Vermi, W., Gilfillan, S., Rossini, C., Cella, M., Barrow, A.D., Diamond, M.S., and Colonna, M. (2012). IL-34 is a tissue-restricted ligand of CSF1R required for the development of Langerhans cells and microglia. Nat. Immunol. *13*, 753–760.

Wang, W.Y., Tan, M.S., Yu, J.T., and Tan, L. (2015). Role of pro-inflammatory cytokines released from microglia in Alzheimer's disease. Ann. Transl. Med. *3*, 136.

Yamasaki, R., Lu, H., Butovsky, O., Ohno, N., Rietsch, A.M., Cialic, R., Wu, P.M., Doykan, C.E., Lin, J., Cotleur, A.C., et al. (2014). Differential roles of microglia and monocytes in the inflamed central nervous system. J. Exp. Med. *211*, 1533–1549.

Yeh, F.L., Wang, Y., Tom, I., Gonzalez, L.C., and Sheng, M. (2016). TREM2 Binds to Apolipoproteins, Including APOE and CLU/APOJ, and Thereby Facilitates Uptake of Amyloid-Beta by Microglia. Neuron *91*, 328–340.

Zhang, Y., Chen, K., Sloan, S.A., Bennett, M.L., Scholze, A.R., O'Keeffe, S., Phatnani, H.P., Guarnieri, P., Caneda, C., Ruderisch, N., et al. (2014). An RNA-sequencing transcriptome and splicing database of glia, neurons, and vascular cells of the cerebral cortex. J. Neurosci. *34*, 11929–11947.

STAR★METHODS

KEY RESOURCE TABLE

REAGENT or RESOURCE	SOURCE	IDENTIFIER
Antibodies		
Amyloid Fibrils OC antibody	Millipore	Cat# AB2286 RRID: AB_1977024
Mouse Amyloid 1-16aa (6e10)	BioLegend	Cat# 803001 RRID: AB_2564653
Mouse β3Tubulin	BioLegend	Cat# 801201 RRID: AB_2313773
Mouse SC121 (human cytoplasm)	Takara Bio	Cat# AB-121-U-050, RRID: AB_2632385
Mouse ku80 (human nuclei)	Abcam	Cat # ab79220, RRID: AB_1603596
Chicken GFAP	Abcam	Cat# ab50738, RRID: AB_880201
Rabbit Iba1	Wako	Cat# 27030, RRID: AB_2314667
Goat Iba1	Abcam	Cat# ab5076, RRID: AB_2224402
Mouse ITGB5	Abcam	Cat# ab177004
Mouse MMP9	Millipore	Cat# AB19016, RRID: AB_11211211
Mouse MERTK	BioLegend	Cat# 367602, RRID: AB_2565898
Rabbit P2RY12	Sigma	Cat# HPA014518
Rabbit PROS1	Abcam	Cat# ab97387, RRID: AB_10695954
Rabbit PU1	Cell Signaling Technology	Cat# 2266S, RRID: AB_10692379
Tabbit TMEM119 (human, C terminus)	Abcam	Cat# ab185333
Goat TREM2 (human)	R&D Systems	Cat# AF1828, RRID: AB_2208689
Rabbit TGFβR1	Abcam	Cat# ab31013, RRID: AB_778352
Rabbit CX3CR1	Bio-Rad/AbD Serotec	Cat# AHP1589, RRID: AB_2087421
LEAF Purified anti-human CD11b	BioLegend	Cat# 301312, RRID: AB_314164
Tau (T22), oligomeric	EMD Millipore	Cat# ABN454
APC-Cyanine7 CD45 (HI30)	Tonbo Biosciences	Cat# 25-0459-T10
PE/Cy7 CD235a (Glycophorin A) (clone HI264)	BioLegend	Cat# 349112, RRID: AB_2562708
APC CD43 Antibody (clone CD43-10G7)	BioLegend	Cat# 343206, RRID: AB_2194072
FITC CD34 Antibody (clone 561)	BioLegend	Cat# 343604, RRID: AB_1732005
PE CD41 Antibody (clone HIP8)	BioLegend	Cat# 303706, RRID: AB_314376
Zombie Violet Fixable Viability Stain	BioLegend	Cat# 423114
Biological Samples		
Human adult microglia RNA	This paper	N/A
Human fetal microglia RNA	This paper	N/A
Human PBMCs	This paper	N/A
Human fetal tissue	This paper	N/A
Chemicals, Peptides, and Recombinant Proteins		
Human TGFβ1	Miltenyi	Cat# 130-108-969
Human IL34	PeproTech	Cat# 200-34
Human MCSF	Thermo Fisher Scientific	Cat# PHC9501
Human FGF2	Thermo Fisher Scientific	Cat# PHG0261
Human BMP4	Thermo Fisher Scientific	Cat# PHC9531
Human Activin A	Thermo Fisher Scientific	Cat# PHC9564
Human TPO	Thermo Fisher Scientific	Cat# PHC9514
Human IL6	Thermo Fisher Scientific	Cat# PHC0061
Human IL3	Thermo Fisher Scientific	Cat# PHC0031
Human VEGF	Thermo Fisher Scientific	Cat# PHC9391

(*Continued on next page*)

Continued

REAGENT or RESOURCE	SOURCE	IDENTIFIER
Human SCF	Thermo Fisher Scientific	Cat# PHC2111
Human Fractalkine (CX3CL1)	PeproTech	Cat# 300-31
Human CD200	Novoprotein	Cat# C311-50ug
BD Matrigel Matrix Growth Factor Reduced, Phenol Red-Free	BD Biosciences	Cat# 356231
TeSR-E8	STEMCELL Technologies	Cat# 05940
IMDM (Iscove's Modified Dulbecco's Medium)	Thermo Fisher Scientific	Cat# 12440053
Ham's F12	Thermo Fisher Scientific	Cat# 11765054
DMEM/F-12, HEPES, no phenol red	Thermo Fisher Scientific	Cat# 11039021
RPMI 1640 Medium, no phenol red	Thermo Fisher Scientific	Cat# 11835030
BSA solution	Miltenyi	Cat# 130-091-376
Lithium Chloride solution	Sigma	Cat# L7026-100ML
L-Ascorbic acid 2-phosphate sesquimagnesium salt hydrate	Sigma	Cat# A8960-5G
1-Thioglycerol (Monothioglycerol)	Sigma	Cat# M1753-100ML
Poly-vinyl-Alcohol (PVA)	Sigma	Cat# P8136-250G
B27 Supplement	Thermo Fisher Scientific	Cat# 17504044
N2 Supplement	Thermo Fisher Scientific	Cat# 17502048
Non-essential Amino Acids (NEAA)	Thermo Fisher Scientific	Cat# 11140050
GlutaMax Supplement	Thermo Fisher Scientific	Cat# 35050061
ROCK inhibitor Y-27632	R&D Systems	Cat# 1254
Human Insulin	Sigma	Cat# I2643-50MG
Insulin-Transferrin-Selenium (ITS-G) (100×)	Thermo Fisher Scientific	Cat# 41400045
Insulin-Transferrin-Selenium-Ethanolamine (ITS-X) (100×)	Thermo Fisher Scientific	Cat# 51500056
Penicillin-Streptomycin	Thermo Fisher Scientific	Cat# 15140122
Adenosine 5′-diphosphate	Sigma	Cat# 01905-250MG-F
PSB 0739	Tocris	Cat# 3983
Fura-2, AM, cell permeant	Thermo Fisher Scientific	Cat# F1201
May-Grünwald Stain	Sigma	Cat# MG1L SIGMA
Giemsa Stain	Sigma	Cat# GS500-500ML
β-Amyloid (1–42), Human	AnaSpec	Cat# AS-20276
β-Amyloid (1–42), HiLyte Fluor 555—labeled, Human	AnaSpec	Cat# AS-60480-01
Human Brain derived Tau Oligomers	This paper	N/A
Human Brain derived Synaptosomes	This paper	N/A
pHrodo Red Dye	Thermo Fisher Scientific	Cat# P36600
RNA-later	Thermo Fisher Scientific	Cat# AM7021
KnockOut Replacement Serum (KOSR)	Thermo Fisher Scientific	Cat# 10828028
Fetal Bovine Serum	Thermo Fisher Scientific	Cat# 10437028
Lipidure-coated 96-well V-bottom plate	AMSBIO	Cat# AMS.51011612
Amylo-Glo RTD Amyloid Plaque Stain Reagent	Biosensis	Cat# TR-300-AG
TrypLE Select Enzyme (1×), no phenol red	Thermo Fisher Scientific	12563029
Critical Commercial Assays		
Human Pluripotent Stem Cell Functional Identification Kit	R&D Systems	Cat# SC027B
V-PLEX Human Cytokine 30-Plex	Meso Scale Discovery	Cat# K15054D-1

(*Continued on next page*)

Continued

REAGENT or RESOURCE	SOURCE	IDENTIFIER
nCounter Human Copy Number Variants	Nanostring	Cat# 115000102
nCounter Human Copy Number Variants Master Kit	Nanostring	Cat# 100052
Kapa Library Quantification Kit	Kappa Biosystems	N/A
TruSeq RNA Library Prep Kit v.2	Illumina	N/A
QIAGEN RNA kit	QIAGEN	Cat# 74106
cDNA kit	Thermo Fisher Scientific	Cat# 11754050
EasySepTM Monocyte Enrichment Kit	STEMCELL Technologies	19059
EasySep Human Pan-DC Pre-Enrichment Kit	STEMCELL Technologies	19251
Deposited Data		
RNA-Seq Data	This paper	GEO: GSE89189
Experimental Models: Cell Lines		
Rat Hippocampal neurons	This paper	N/A
Commercial iHPCs (Lot# 021405)	Cellular Dynamics International	Cat# HPC-301-020-001-PT
Human: iPSC line from Fibroblast: Male	UCI ADRC iPSC Core	ADRC 2
Human: iPSC line from Fibroblast: Male	UCI ADRC iPSC Core	ADRC 4
Human: iPSC line from Fibroblast: Female	UCI ADRC iPSC Core	ADRC 5
Human: iPSC line from PBMC: Male	UCI ADRC iPSC Core	ADRC 12
Human: iPSC line from Fibroblast: Male	UCI ADRC iPSC Core	ADRC F14
Human: iPSC line from Fibroblast: Female	UCI ADRC iPSC Core	ADRC 20
Human: iPSC line from PBMC: Female	UCI ADRC iPSC Core	ADRC 22
Human: iPSC line from PBMC: Male	UCI ADRC iPSC Core	ADRC 76
Human: iPSC line from Fibroblast: Male	UCI ADRC iPSC Core	ADRC 85
Human: iPSC line from Fibroblast: Female	UCI ADRC iPSC Core	ADRC 86
Human: fetal-derived microglia: sex N/A	This paper	N/A
Human: Monocytes—Sex in Method Details	This paper	N/A
Human: Monocyte-derived macrophages	This paper	N/A
Human: Blood-borne Dendritic Cells Sex in Method Details	This paper	N/A
Human: iPSC-derived HPCs	This paper	N/A
Experimental Models: Organisms/Strains		
Rag-5xfAD; mouse: B6.Cg-Tg (APPSwFlLon,PSEN1*M146L*L286V) 6799Vas/Mmjax crossed with mouse: B10;B6-*Rag2*^{tm1Fwa} *Il2rg*^{tm1Wjl} From Jackson Laboratory and Taconic, respectively	Blurton-Jones lab, UC Irvine, CA	Marsh et al., 2016
MITRG; mouse M-CSF^{h};IL-3/GM-CSF^{h};THPO^{h};Rag2^{-};γc^{-}	The Jackson Laboratory	Jax: 017711
Rat: Sprague Dawley Crl:SD	Charles River	Charles River strain code: 400
Oligonucleotides		
Primers for qPCR, see Table S7	Thermo Fisher Scientific	see Table S7
Software and Algorithms		
STAR	Dobin et al., 2013	https://github.com/alexdobin/STAR
RSEM	Li and Dewey, 2011	https://deweylab.github.io/RSEM/
EdgeR	Robinson et al., 2010	http://bioconductor.org/packages/release/bioc/html/edgeR.html
Rstudio	N/A	https://www.rstudio.com/

(*Continued on next page*)

Continued

REAGENT or RESOURCE	SOURCE	IDENTIFIER
Java Tree View 3.0	N/A	http://bonsai.hgc.jp/~mdehoon/software/cluster/software.htm
Enrichr	Chen et al., 2013; Kuleshov et al., 2016	http://amp.pharm.mssm.edu/Enrichr/
FlowJo v.10.0	N/A	https://www.flowjo.com/solutions/flowjo
GraphPad Prism v.7	N/A	https://www.graphpad.com/scientific-software/prism/
Other		
BD FACSARIA Fusion	BD Biosciences	equipment
Amnis ImageStreamX Mark II Image Flow Cytometer	EMD Millipore	equipment

CONTACT FOR REAGENT AND RESOURCE SHARING

Further information and requests for resources and reagents should be directed to and will be fulfilled by the Lead Contact, Mathew Blurton-Jones, PhD (mblurton@uci.edu).

EXPERIMENTAL MODEL AND SUBJECT DETAILS

Chemical Reagents

All cell culture flasks, reagents, supplements, cytokines, and general reagents were purchased from Thermo Fisher Scientific, unless otherwise noted.

Cell Culture

Maintenance and Culture of Human Pluripotent Stem Cells (hPSCs)

All stem cell work was performed with approval from UC Irvine Human Stem Cell Research Oversight (hSCRO) and IBC committees. The use of human fibroblast and PBMC samples for iPSC reprogramming and differentiation was approved by the University of California, Irvine Institutional Review Board (IRB Protocol #2013-9561) and informed consent was obtained from all subjects. Human iPSC cell lines ADRC 2 (Male), 4 (Male), 5 (Female), 12 (Male), 14 (Male), 20 (Female), 22 (Female), 76 (Male), 85 (Female), and 86 (Female) were generated by the UCI Alzheimer's Disease Research Center (ADRC) Induced Pluripotent Stem Cell Core using non-integrating Sendai virus (Cytotune) and are available to other researchers via http://stemcells.mind.uci.edu/. iPSCs were confirmed to be sterile and karyotypically normal via G-banding (http://www.WiCell.org). Pluripotency of all lines was confirmed via (http://pluritest.org) and further confirmed using the Human Pluripotent Stem Cell Functional Identification Kit (R&D Systems), per manufacturer's instructions.

iPSCs were maintained in 6-well plates (Corning) in feeder-free conditions using growth factor-reduced Matrigel (MTG, BD Bioscience) in complete TeSR-E8 medium (STEMCELL Technologies) in a humidified incubator (5% CO_2, 37°C). iPSCs were fed fresh media daily and passaged every 7-8 days.

Differentiation of iPSCs to Hematopoietic Progenitor Cells

Human iPSC-derived hematopoietic progenitors were generated using defined conditions with several modifications to previously published protocols (Kennedy et al., 2007; Sturgeon et al., 2014).

iHPC Differentiation Base Medium Formulation: IMDM (50%), F12 (50%), insulin (0.02 mg/ml), holo-transferrin (0.011 mg/ml), sodium selenite (13.4 μg/ml), ethanolamine (4 μg/ml) (can use ITSG-X, 2% v/v, Thermo Fisher Scientific), L-ascorbic acid 2-Phosphate magnesium (64 μg/ml; Sigma), monothioglycerol (400 μM), PVA (10 μg/ml; Sigma), Glutamax (1X), chemically-defined lipid concentrate (1X), non-essential amino acids (NEAA; 1X), Penicillin/Streptomycin (P/S; 1% V/V). Use 0.22 μm filter.

Day (−1): iPSCs were washed with room temperature 1X DPBS (minus Ca^{2+} and Mg^{2+}) once. Wash was aspirated to waste and TrypLE Select (1X; 37°C; 1 mL per 6-well) and placed in incubator (5% CO_2, 37°C). After 3-5 min, cells were placed in cell culture hood and the side of the plate was lightly tapped for 30 s to dislodge iPSCs. After lightly tapping the plate, 1 mL of room temperature 1X DPBS (minus Ca^{2+} and Mg^{2+}) was added to each well. Then cells were collected into a 15 mL conical tube (Corning) using a 10 mL Stripette (Corning). Cells were centrifuged at 200 x *g* for 5 min at room temperature. After centrifugation, supernatant was aspirated to waste and cells were suspended in E8 medium + Y-27632 ROCK Inhibitor (RI,10 μM; R&D Systems), and gently triturated to generate a single-cell suspension, counted, and cell density adjusted to seed at 5×10^5 cells/cm^2 in tissue-culture treated 6-well plates. The final volume was adjusted to 1.5 mL of E8+ RI per well. Cells were cultured for 24 hr under normoxic conditions (20% O_2, 5% CO_2, 37°C).

Day (0): Cells were gently collected into a 50 mL conical tube (Corning) using 10 mL Stripette and centrifuged at 300 x *g* for 6 min at room temperature (all media changes will require this step using these parameters.). Media was aspirated to waste, and media was

changed to basal medium complete with FGF2 (50 ng/ml), BMP4 (50 ng/ml), Activin-A (12.5 ng/ml), RI (1 μm) and LiCl (2mM) at 2 mL per well. Cells were then placed in humidified tri-gas incubator under hypoxic cell culture conditions (5%O_2, 5%CO_2, 37°C).

Day (2): Cells were quickly and gently collected into a 50 mL conical using 10 mL Stripette and centrifuged. Supernatant was aspirated to waste and media was changed to pre-equilibrated (at 5%O_2, 5%CO_2, 37°C for 1 hr) base media supplemented with FGF2 (50 ng/ml) and VEGF (50 ng/ml) and returned to the hypoxia incubator.

Day (4): Media was changed to 2 mL per well with basal media containing FGF2 (50 ng/ml), VEGF (50 ng/ml), TPO (50 ng/ml), SCF (10 ng/ml), IL-6 (50 ng/ml), and IL-3 (10 ng/ml) and placed into a normoxia incubator.

Days (6 and 8): Cells were supplemented with 1ml per well of Day 4 medium.

Day (10): Cells were collected and prepped for FACS (see Method Details) and $CD43^+$ cells were isolated by FACS for iMGL differentiation. Additionally, iPSC-derived HPCs (Cellular Dynamics International) were identified as a commercial source of $CD43^+$ progenitors.

Differentiation of iHPCs to iMGLs

iMGL Differentiation Base Medium: Differentiation media consists a base media: phenol-free DMEM/F12 (1:1), insulin (0.02 mg/ml), holo-transferrin (0.011 mg/ml), sodium selenite (13.4 μg/ml) (can use ITS-G, 2%v/v, Thermo Fisher Scientific), B27 (2% v/v), N2 (0.5%, v/v), monothioglycerol (200 μM), Glutamax (1X), NEAA (1X), and additional insulin (5 μg/ml; Sigma) and filtered through a 0.22 μm filter.

Day (0; or day 10 from iPSC): Isolated $CD43^+$ iHPCs were washed using iMGL base differentiation medium and centrifuged at 300 x *g* for 6 min at room temperature. After centrifugation, supernatant was aspirated to waste and iHPCs were gently suspended in complete differentiation medium: M-CSF (25 ng/ml), IL-34 (100 ng/ml; PeproTech), and TGFβ-1 (50 ng/ml; Militenyi) added fresh each time. Cell density was adjusted to seed at 1-2 x10^5 cells in 2 mL of complete medium per well in growth factor-reduced Matrigel-coated 6-well plates.

Every two days: Each well was supplemented with 1 mL per well of complete differentiation medium.

Day (12; or day 22 from iPSC): Early iMGLs were collected (300x *g* for 6 min at room temperature) and a 50% media change was performed.

After 25 days of microglial differentiation (35 days from iPSC), iMGLs were cultured in complete differentiation media supplemented with CD200 (100 ng/ml, Novoprotein) and CX3CL1 (100 ng/ml; PeproTech) for an additional three days.

Human Adult and Fetal Microglia Isolation

All studies using human tissue were approved by the McGill University institutional review board (McGill University Health Centre Ethics Board; #ANTJ2001/1). All experiments were conducted in accordance with the Helsinki Declaration. Sex of donor was either not provided or collected. Human microglia were isolated from adult brain tissue using previously described protocols (Durafourt et al., 2013). Briefly, normal appearing cortical tissue was resected from pharmacologically intractable non-malignant cases of temporal lobe epilepsy. Tissue was cleaned extensively and mechanically dissociated. A single cell suspension was generated following gentle enzymatic digestion using trypsin and DNase prior to passing through a nylon mesh filter. Single cell suspension underwent a fickle ultracentrifugation step to remove myelin. Dissociated cells were centrifuged, counted, and plated at 2x10^6 cells/mL in MEM supplemented with heat-inactivated FBS (5%), P/S (0.1% v/v) and glutamine (0.1% v/v.). Microglia were grown for 3 days, collected and plated at 1x10^5 cells/mL and maintained in culture for 6 days during which time cells received two treatments of TGFβ (20 ng/mL) on days 3 and 5. Human fetal brain tissue was obtained from the Fetal Tissue Repository (Albert Einstein College of Medicine, Bronx, NY). Total RNA was isolated using standard Trizol (Thermo Fisher Scientific) protocols and stored at −80°C.

3D Brain-Organoid Generation

Human 3D brain organoids were generated as previously described, with some modifications (Lancaster et al., 2013). iPSCs were cultured and maintained on Vitronectin XF (STEMCELL Technologies) in 6-well tissue culture treated plates (BD Falcon) and maintained with TeSR-E8 media (STEMCELL Technologies) daily, at 37°C with 5% CO_2. At approximately 80% confluency, iPSCs were detached from the Vitronectin XF substrate using the standard ReLeSR protocol (STEMCELL Technologies) and centrifuged, pelleted, and suspended in embryoid body (EB) media, which consists of KO DMEM/F12 (Invitrogen), KOSR (20% v/v), Glutamax (1X), NEAA (1X), 2-Mercaptoethanol (0.1mM), bFGF (4 μg/ml), and HSA (0.1% v/v) and ROCK inhibitor (50 μM), to form EBs. Approximately 1x10^4 cells were plated per well of a standard V-bottom 96-well plate coated with Lipidure (1% v/v; AMSBio) to avoid having the EBs attach to the 96-well plate. After 4 days in EB media with bFGF (4 ng/ml) and ROCK inhibitor (50 μM), both the bFGF and ROCK inhibitor were discontinued leaving the brain organoids in basic EB media for an additional 3 days (7 days total). After the EB media phase, the EB media is replaced with neural epithelium (NE) media which consists of DMEM/F12, N2 supplement (0.1% v/v), Glutamax (1X), MEM-NEAA (0.1X), Heparin solution (0.2mg/ml; Sigma), and filtered using 0.22 μm PES filter (EMD Millipore). The brain organoids were transferred to an ultra-low attachment 24-well plate (Corning) using cut P200 pipette tips, with 1-2 EBs per well in 1 mL NE media. The EBs were neuralized in the NE media for five days, after which they were transferred into Matrigel (Corning) using a mold created from siliconized parafilm and a sterile empty P200 box. The brain organoids were kept in a 6-cm suspension petri dish with differentiation media consisting of KO DMEM/F12 (50%), Neurobasal medium (50%), N2 supplement (0.1% v/v), B27 without vitamin A supplement (0.1% v/v), Insulin solution (0.1% v/v; Sigma), 2-Mercaptoethanol (0.1mM), Glutamax (1X v/v), MEM-NEAA (1X), and Penicillin/Streptomycin (0.1% v/v). After five days of being exposed to differentiation media containing B27 without vitamin A, the differentiation media was replaced by a formulation that is identical except for the replacement of B27 without vitamin A to B27 with vitamin A; at this time point, the brain organoids are also transferred to a 125 mL spinning flask

bioreactor (Corning) siliconized with Sigmacote (Sigma), where they were fed differentiation media with vitamin A weekly for 8 weeks. After 12 weeks, Borgs were utilized for iMGL co-culture studies.

Rat Cortical and Hippocampal Neuron Isolation

All procedures were performed under an IUCAC approved protocol. Primary cortical and hippocampal neuron cultures were derived from embryonic rat (E18) as previously described (Loo et al., 1993). Briefly, dissected tissue was dissociated with trypsin, triturated, and plated on 6-well plates coated with poly-L-lysine coated in NB medium (serum-free Neurobasal supplemented with 1% B27). Cells were plated at a density of 5×10^6 cells/ml and cells were fed once a week with 50% media change until used for assays.

PBMCs and Monocytes Isolation from Human Blood

The isolation of human monocytes and dendritic cells from de-identified human subjects was performed under IRB Protocol #2015-2437 and through the UC Irvine ICTS Blood Donor Program. Donor sex: CD14 M = 2 males, 3 females. CD16 M = 2 males, 2 females. Blood DCs were all from female donors. Peripheral blood mononuclear cells (PBMCs) were isolated from healthy donors using Ficoll-paque (GE Healthcare) gradient separation. In brief, blood was layered on top of Ficoll-Paque and centrifuged in swinging bucket rotator without brake (400x *g*, 40 min, 18°C). After centrifugation, plasma and upper layers were removed and PBMCs isolated from the interphase. Cells were then washed once with ice-cold PBS and used immediately. CD14 and CD16 monocytes were isolated via negative selection from PBMCs using the EasySep Monocyte Enrichment Kit (STEMCELL Technologies) per manufacturer's instructions. Blood dendritic cells were isolated via negative selection from PBMCs using the EasySep Human Pan-DC Pre-Enrichment Kit (STEMCELL Technologies) per manufacturer's instructions. Isolated cells were washed three times with PBS and sorted by FACS for either RNA-sequence analysis or used for further macrophage differentiation.

Monocyte-Derived Macrophages

Isolated monocytes (from males) were plated onto tissue culture treated 6-wells at 2 $x10^6$ cells/ml in RPMI-1640 media at 37°C 5% CO_2 incubator. After two hours, media was aspirated to waste and adherent monocytes washed three times with DPBS and replaced with complete media composed of RPMI-1640, FBS (10% v/v), Penicillin/streptomycin (1% v/v), Glutamax (1X). To generate MD-Mϕ, M-CSF (25 ng/ml) was added to wells and cells differentiated for 5 days.

METHOD DETAILS

RNA-Seq Library Construction

Cells were harvested and washed three times with DPBS and stored in RNAlater, RNA preservation solution. RNA was extracted from all cell types using RNeasy Mini Kit (QIAGEN) following manufacturer's guidelines. RNA integrity (RIN) was measured for all samples using the Bioanalzyer Agilent 2100 series. All sequencing libraries analyzed were generated from RNA samples measuring a RIN score $\geq$ 9. The Illumina TruSeq mRNA stranded protocol was used to obtain poly-A mRNA from all samples. 200 ng of isolated mRNA was used to construct RNA-seq libraries. Libraries were quantified and normalized using the Library Quantification Kit from Kapa Biosystems and sequenced as paired-end 100 bp reads on the Illumina HiSeq 2500 platform.

Confocal Microscopy and Bright-Field Imaging

Immunofluorescent sections were visualized and images captured using an Olympus FX1200 confocal microscope. To avoid non-specific bleed-through, each laser line was excited and detected independently. All images shown represent either a single confocal *z*-slice or *z*-stack. Bright-field images of cell cultures were captured on an Evos XL Cell Imaging microscope. Image analysis was performed using Olympus.

FACS and Flow Cytometer Analysis

iHPCs were collected using cold (4°C) sterile filtered and degassed FACS buffer (1X DPBS, 2% BSA, and 0.05mM EDTA) spiked with human SCF (5 ng/ml). Cells were then filtered through 70 μm mesh to remove large clumps, washed with spiked FACS buffer (300 x *g* for 5 min 18°C), then stained (1:200) using spiked FACS buffer on ice for 1 hr in the dark using the following antibodies: anti CD34-FITC clone 561, anti CD41-PE clone HiP8, anti CD43-APC clone CD43-10G7, anti CD45-APC/Cy7 clone HI30 (Tonbo Biosciences), anti CD235a-PE/Cy7 clone HI264, and ZombieViolet live/dead stain, all from BioLegend unless noted. After staining, iHPCs were washed once with spiked FACS buffer and suspended using spiked FACS buffer (500-700 μl) and sorted utilizing the BD FACSARIA Fusion (BD Biosciences). Sorted cells were collected in cold basal iHPC differentiation medium spiked with SCF (10 ng/ml). Collected CD43+ iHPCs were then plated for iMGL differentiation as mentioned above. iMGLs were suspended in FACS buffer and incubated with human Fc block (BD Bioscience) for 15 min at 4°C. For detection of microglial surface markers, cells were stained with anti CD11b-FITC clone ICRF44, anti CD45-APC/Cy7 clone HI30 (Tonbo Biosciences), anti CX3CR1-APC clone 2A9-1, anti CD115-PE clone 9-4D, and anti CD117-PerCP-Cy5.5 clone 104D2, ZombieViolet live/dead stain, all from BioLegend. Cells were sorted on a FACS Aria II, FACS Aria Fusion (BD Biosciences) and data analyzed with FlowJo software (FlowJo).

Cytospin and May-Grunwald Giemsa Stain

$1x10^5$ cells were suspended in FACS buffer (100 μl) and added to Shandon glass slides (Biomedical Polymers) and assembled in a cytology funnel apparatus. Assembled slides containing cells were loaded in a cytospin instrument and centrifuged (500 rpm, 5 min). Slides were allowed to air-dry for two minutes and immediately stained in May-Grunwald stain (100%; Sigma) for 5 min. Next, slides

were washed in PBS for 1.5 min and immediately placed in Giemsa stain (4%; Sigma) for 20 min at room temperature. Slides were washed in double-distilled water 6 times and allowed to air-dry for 10 min. Slides were preserved using glass coverslips and permount (Sigma).

RNA Isolation and qPCR Analysis

Cells were stored in RNAlater stabilizing reagent and RNA was isolated using QIAGEN RNeasy Mini Kit (Valencia, CA) following manufacturer's guidelines. qPCR analysis was performed using a ViiA 7 Real-Time PCR System and using Taqman qPCR primers. Analysis of AD-GWAS genes utilized a custom Taqman Low Density Array card using the primers described below.

iMGL Co-culture with Rat Neurons

Rat hippocampal or cortical neurons were cultured for 21 days with 50% media change every 3-4 days. iMGLs were cultured with neurons at a 1:5 ratio (1 x10^6 iMGL to 5 × 10^6 neurons) in 50% iMGL and 50% NB medium. After 3 days, iMGLs were collected for RNA isolation.

iMGL Transplantation in MITRG and Rag-5xfAD Brains

All animal procedures were performed in accordance with NIH and University of California guidelines approved IAUC protocols (IAUC #2011-3004). MITRG mice were purchased from Jax (The Jackson Laboratory, #017711) and have been previously characterized (Rongvaux et al., 2014). MITRG mice allow for xenotransplantation and is designed to support human myeloid engraftment. iMGLs were harvested at day 38 and suspended in injection buffer: 1X HBSS with M-CSF (10 ng/ml), IL-34 (50 ng/ml), and TGFβ-1 (25 ng/ml). iMGLs were delivered using stereotactic surgery as previously described (Blurton-Jones et al., 2009) using the following coordinates; AP: −0.6, ML: ± 2.0, DV: −1.65. Brains were collected from mice at day 60 post-transplantation per established protocols (Blurton-Jones et al., 2009). Rag-5xfAD mice were generated in this lab and previously characterized (Marsh et al., 2016). Rag-5xfAD mice display robust beta-amyloid pathology and allow for xenotransplantation of human cells. iMGLs were transplanted into the hippocampi using the following coordinates; AP: −2.06, ML: ± 1.75, DV: −1.95. After transplantation mice were killed and brains collected using previously established protocol. Briefly, mice were anesthetized using sodium-barbiturate and perfused through the left-ventricle with cold 1X HBSS for 4 min. Perfused mice were decapitated and brain extracted and dropped-fixed in PFA (4% w/v) for 48 hr at 4°C. Brains were then washed 3 times with PBS and sunk in sucrose (30% w/v) solution for 48 hr before coronal sectioning (40 μm) using a microtome (Leica). Free-floating sections were stored in PBS sodium azide (0.05%) solution at 4°C until IHC was performed.

Immunocytochemistry and Immunohistochemistry

For ICC, cells were washed three times with DPBS (1X) and fixed with cold PFA (4% w/v) for 20 min at room temperature followed by three washes with PBS (1X). Cells were blocked with blocking solution (1X PBS, 5% goat or donkey serum, 0.2% Triton X-100) for 1 hr at room temperature. ICC primary antibodies were added at respective dilutions (see below) in blocking solution and placed at 4°C overnight. The next day, cells were washed 3 times with PBS for 5 min and stained with Alexa Fluor conjugated secondary antibodies at 1:400 for 1 hr at room temperature in the dark. After secondary staining, cells were washed 3 times with PBS and coverslipped with DAPI-counterstain mounting media (Fluoromount, southern Biotech). For BORG IHC, tissue were collected and dropped-fixed in PFA (4% w/v) for 30 min at room temperature and then washed three times with PBS. BORGs were then placed in sucrose solution (30% w/v) overnight before being embedded in O.C.T (Tissue-Tek). Embedded tissue was sectioned at 20 μm using a cryostat and mounted slides were stored at −20°C until staining. For BORG staining, mounted tissue was removed from storage and warmed by placing at room temperature for 30 min. Tissue were rehydrated and washed with room temperature PBS (1X) 3 times for 5 min. Heat-mediated antigen retrieval was performed by using Citrate Buffer (10mM Citrate, 0.05% Tween 20, pH = 6.0) at 97°C for 20 min and then allowed to cool to room temperature. After antigen retrieval, slides were washed three times with PBS. Slides were then washed once in PBS-A solution (1X PBS with 0.1% Triton X-100) for 15 min. Tissue was blocked using PBS-B solution (PBS-A, 0.2% BSA, and 1.5% goat or donkey serum) for 1 hr at room temperature. After block, primary antibodies were added to PBS-B solution (250-350 μl/ slide) at appropriate dilutions (see below) and incubated overnight at room temperature. The next day, slides were washed with PBS-A solution 3 times for 5 min each. Tissue were blocked for 1 hr using PBS-B solution at room temperature. After block, slides were incubated with Alexa Fluor conjugated secondary antibodies (all at 1:500) and Hoechst stain (1X) in PBS-B (for 250-300 μl/slide) for 2 hr at room temperature in the dark. After secondary staining, slides were washed 5 times with PBS for 5 min. Slides were coverslipped using fluoromount (Southern Biotech). For mouse brain IHC, brains were collected, fixed, and processed as mentioned above. Free-floating sections were blocked in blocking solution (1X PBS, 0.2% Triton X-100, and 10% goat serum) for 1 hr at room temperature with gentle shaking. For human TMEM119 staining, heat mediated antigen retrieval was performed prior to blocking, as performed previously (Bennett et al., 2016). Free-floating tissue antigen retrieval was performed by placing floating sections in a 1.5 mL micro centrifuge tube containing 1 mL of Citrate Buffer solution and placing in a pre-heated temperature block set at 100°C. Tissue was heated for 10 min at 100°C then removed and allowed to come to room temperature for 20 min before washing with PBS 3 times for 5 min and then proceeding with blocking step. For AD mouse brain staining of amyloid plaques, floating sections were placed in 1X Amylo-Glo RTD (Biosensis) staining solution for 10 min at room temperature without shaking. After staining, sections were washed in PBS 3 times for 5 min each and briefly rinsed in MiliQ DI water before being placed

back in to PBS followed by blocking. Primary antibodies were added to staining solution (1X PBS, 0.2% Triton X-100, and 1% goat serum) at appropriate dilutions (see below) and incubated overnight at 4°C with slight shaking. The next day, sections were washed 3 times with PBS and stained with Alexa Fluor conjugated secondary antibodies at 1:400 for 1 hr at room temperature with slight shaking in the dark. After secondary staining, sections were washed in PBS 3 times for 5 min and mounted on glass slides. After mounting, slides were coverslipped with DAPI-counterstain mounting media (Fluoromount, southern Biotech). Primary antibodies: mouse anti-β3Tubulin (1:500; BioLegend, 801201), mouse anti-human Cytoplasm (SC121,1:100; Takara Bio, Y40410), mouse anti-human Nuclei (ku80, 1:100; Abcam, ab79220), chicken anti-GFAP (1:500; Abcam, ab4674), rabbit anti-Iba1 (1:500; Wako; 019-19741), goat anti-Iba1 (1:100; Abcam ab5076) (recommend use with Alexa Fluor 488 or 555 secondary antibody only), mouse anti-ITGB5 (1:500; Abcam, ab177004), mouse anti-MMP-9 (1:500; EMD Millipore, AB19016), mouse anti-human Mertk (1:500; BioLegend, 367602), rabbit anti-P2ry12 (1:125; Sigma; HPA014518), rabbit anti-Pros1 (1:500; Abcam, ab97387), rabbit anti-PU.1 (1:500; Cell Signaling Technology, 2266S), rabbit anti-human Tmem119 (1:100; Abcam, ab185333), goat anti-human Trem2 (1:100; R&D Systems, AF1828), rabbit anti-Tgfbr1 (1:500; Abcam, ab31013), rabbit anti-Cx3cr1 (1:1000; Bio-Rad/AbD Serotec, AHP1589). Other primary antibodies used: rabbit anti-Amyloid Fibrils (OC) (1:1,000, EMD Millipore, AB2286), rabbit anti-Amyloid Oligomeric (A11) (1:1,000, EMD Millipore, AB9234), mouse anti-Amyloid 1-16aa (6e10) (1:1,000, BioLegend, 803001).

ADP Migration and Calcium Imaging Assays

Trans-well migration assays to ADP was performed as previously described (De Simone et al., 2010; Moore et al., 2015). iMGLs ($5.5x10^4$ cells/well) were cultured in serum-free basal media without cytokines pre-exposed to DMSO or PSB0739 (50 μM, Tocris) for 1hr at 37°C in 5% CO_2 cell culture incubator. Cells were then washed three times with basal medium and plated in *trans*-well migration chambers (5 μm polycarbonate inserts in 24 wells; Corning) containing Adenosine 5′-phosphate (ADP, 100 μM; Sigma) in the bottom chamber in 37°C in 5% CO_2. After 4 hr, cells were washed three times with PBS (1x) and fixed in PFA (4%) for 15 min at room temperature. Cells were stained with Hoechst stain for 10 min to visualize nuclei of cells. A blinded observer counted total cells per slide and then scrubbed cells off top surface using a cotton-swab, washed with PBS, and recounted to record migrated cells. Migration was reported as migrated over total cells per well. Fluorescent images of cells were captured using Olympus IX71 inverted microscope.

For calcium imaging, iMGLs were plated on poly-L-lysine-coated coverslips and 1 hr later were incubated with Fura-2-AM (Molecular Probes) calcium dye diluted in Ringer solution containing (in mM): NaCl 140, KCl 4.5, $CaCl_2$ 2, $MgCl_2$ 1, HEPES 10, glucose 10, sucrose 5, pH = 7.4. After 1 hr incubation, the dye was washed out 3 times using Ringer solution and treated for 1 hr with either P2ry12 inhibitor PSB0739 (50 μM, Tocris) or Vehicle (DMSO) and used for experiments. Baseline Ca^{2+} signal (I_{340}/I_{380}) were measured for more than 100 s and then ADP (10 μM) was introduced under steady flow after baseline measurement. Ca^{2+} recordings were performed on Zeiss (Axiovert 35)-based imaging setup and data acquisition was conducted with Metafluor software (Molecular Devices). Data analysis was performed using Metafluor, Origin Pro, and Prism 6.0.

Phagocytosis Assays

iMGLs and MD-Mϕ, were incubated with mouse anti CD16/32 Fc-receptor block (2 mg/ml; BD Biosciences) for 15 min at 4°C. Cells were then stained with anti CD45-APC clone HI30 (Tonbo Biosciences) at 1:200 in flow cytometer buffer. Samples were then analyzed using Amnis ImageStreamerX Mark II Imaging Flow Cytometer (Millipore). *E.coli*, human synaptosome, fAβ, and BDTO phagocytosis was analyzed using the IDEAS software onboard Internalization Wizard algorithm. Additive free Anti-CD11b antibody (BioLegend, #301312) was used for CD11b blockade.

Fibrillar Aβ Preparation

Fibrillar fluorescent amyloid-beta ($fA\beta_{1-42}$) was generated as described previously (Koenigsknecht-Talboo and Landreth, 2005). Fluorescently labeled Aβ peptide (AnaSpec; Fremont, CA) was first dissolved in NH_4OH (0.1%) to 1 mg/ml, then further diluted to 100 μg/ml using sterile endotoxin-free water, vortexed thoroughly, and incubated at 37°C for 7 days. fAβ was thoroughly mixed prior to cell exposure.

BDTO Preparation

Brain-derived tau oligomers were purified by immunoprecipitation as described previously (Lasagna-Reeves et al., 2012). Tau oligomers were isolated by immunoprecipitation with the T22 antibody using PBS-soluble fractions of homogenates prepared from AD brain. These were then purified by fast protein liquid chromatography (FPLC) using PBS (pH 7.4). Additional analyses include western blots to detect contamination with monomeric tau or large tau aggregates (tau-5, normally appear on top of the stacking gel) and using a mouse anti-IgG to identify non-specific bands. BDTOs were subsequently conjugated to pHrodo-Red per manufacturer's protocol.

Human Synaptosomes

The synaptosome preparation protocol was adapted from (Gylys et al., 2000). Human tissue samples were obtained at autopsy and minced, slowly frozen in 0.32 M sucrose with 10% DMSO and stored at −80 °C. To obtain a crude synaptosome fraction, tissue was thawed in a 37 °C water bath and homogenized in 10 mm Tris buffer (pH 7.4) with proteinase inhibitors (Roche) and phosphatase

inhibitors (Sigma-Aldrich) using a glass/Teflon homogenizer (clearance 0.1–0.15 mm). The homogenate was centrifuged at 1000 *g* at 4 °C for 10 min, the supernatant was removed and centrifuged again at 10,000 *g* at 4 °C for 20 min. Resulting pellets were suspended in sucrose/Tris solution and stored at −80 °C. Synaptosomes were conjugated to pHrodo-Red per the manufacturer's protocol.

Mesoscale Multiplex Cytokine and Chemokine Assay

iMGL culture media was replaced with basal media for 2 hr prior to stimulation with IFNγ (20 ng/ml), IL1β (20 ng/ml), and LPS (100 ng/ml) for 24 hr, after which cells were collected for RNA and conditioned media assessed for cytokine secretion. To simultaneously assess multiple cytokine and chemokine analytes from iMGL conditioned media, conditioned media from each treatment group was processed and analyzed using the V-PLEX human cytokine 30-plex kit (Mesoscale) per the manufacturer's protocol.

Dot Blot

Serial dilutions of proteins (2 μl) were blotted on a pre-wet nitrocellulose paper and allowed to dry. After drying, blots were blocked with 5% BSA in 1x Tris-buffered saline with Tween 20 (TBST) for 1 hr at room temperature with slight shaking. Next, blots were incubated with primary antibodies (see below) at room temperature for 1 hr. Blots were then washed 3 times for 5 min each with TBST. Blots were then incubated with HRP conjugated secondary antibody (Santa Cruz) at 1:10,000 for 1 hr at room temperature with mild shaking. After 1 hr, blots were washed 3 times for 5 min each with TBST. After wash, blots were dried on filter paper and incubated with Pierce ECL western blotting development substrate (Thermo Fisher Scientific) for 10 min in the dark. Blots were imaged on ChemiDoc XRS+ imaging system (Bio-Rad).

AD-GWAS qPCR Primers

The following validated and available Taqman primers were used: APOE Hs00171168_m1, CR1 Hs00559342_m1, CD33 Hs01076281_m1, ABCA7 Hs01105117_m1, TREM2 Hs00219132_m1, TREML2 Hs01077557_m1, TYROBP (DAP12) Hs00182426_m1, PICALM Hs00200318_m1, CLU Hs00156548_m1, MS4A6A Hs01556747_m1, BIN1 Hs00184913_m1, CD2AP Hs00961451_m1, CASS4 Hs00220503_m1, MEF2C Hs00231149_m1, DSG2 Hs00170071_m1, MS4A4A Hs01106863_m1, ZCWPW1 Hs00215881_m1, INPP5D Hs00183290_m1, and PTK2B Hs00169444_m1.

QUANTIFICATION AND STATISTICAL ANALYSIS

RNA-Seq Analysis

RNA-seq reads were mapped to the hg38 reference genome using STAR (Dobin et al., 2013) aligner and mapped to Gencode version 24 gene annotations using RSEM (Li and Dewey, 2011). Genes with expression (< 1 FPKM) across all samples were filtered from all subsequent analysis. Differential gene expression analysis was performed on TMM normalized counts with EdgeR (Robinson et al., 2010). Multiple biological replicates were used for all comparative analysis. A p value $\leq$ 0.001 and a 2-fold change in expression were used in determining significant differentially expressed genes for respective comparisons. PCA analysis was performed using the R package "rgl" and plotted using "plot3d." Clustering was performed using R "hclust2" and visualized using Java Tree View 3.0 (http://bonsai.hgc.jp/~mdehoon/software/cluster/software.htm). Differential gene analysis between groups was performed using the R package "limma" and significant genes (adjusted $p < 0.01$) were used for Gene ontology and pathway analysis. Gene ontology and pathway analysis was performed using Enrichr database (http://amp.pharm.mssm.edu/Enrichr/) (Chen et al., 2013; Kuleshov et al., 2016).

Statistical Analysis

Statistical analysis was performed using Graphpad Prism 7 software. Comparisons involving more than two groups utilized one-way ANOVA followed by Tukey's post hoc test and corrected p values for multiple comparisons were reported. Comparison's with more than two groups and comparing to a control or vehicle group utilized one-way ANOVA followed by Dunnett's post hoc test with corrected p values for multiple comparisons reported. Two-Way ANOVA were followed by Sidak's multiple-comparison post hoc test Comparisons of two groups utilized two-tailed Students t test. All differences were considered significantly different when $p < 0.05$. Statistical analysis for RNA-sequencing is detailed above and all further statistical analysis details are reported in the figure legends.

DATA AND SOFTWARE AVAILABILITY

Raw and normalized RNA sequence data can be obtained at NCBI. The GEO Accession Super Series ID number for the data reported in this paper is GEO: GSE89189.